Distributed Tertiary Control of DC Microgrid Clusters

Seyedali Moayedi, *Student Member, IEEE*, and Ali Davoudi, *Member, IEEE*

***Abstract*—A distributed control method is proposed to handle power sharing among a cluster of dc microgrids. The hierarchical control structure of microgrids includes primary, secondary, and tertiary levels. While the load sharing among the sources within a dc microgrid is managed through primary and secondary controllers, a tertiary control level is required to provide the higher level load sharing among microgrids within a cluster. Power transfer between microgrids enables maximum utilization of renewable sources and suppresses stress and aging of the components, which improves its reliability and availability, reduces the maintenance costs, and expands the overall lifespan of the network. The proposed control mechanism uses a cooperative approach to adjust voltage set points for individual microgrids and, accordingly, navigate the power flow among them. Loading mismatch among neighbor microgrids is used in an updating policy to adjust voltage set point and mitigate such mismatches. While the voltage adjustment policy handles the load sharing among the microgrids within each cluster, at a lower level, each microgrid carries a communication network that is in contact with the secondary control system. It is this lower level network that propagates voltage set points across all sources within a microgrid. Load sharing and set point propagation are analytically studied for the higher and lower level controllers, respectively. Experimental studies on two cluster setups demonstrate excellent controller performance and validate its resiliency against converter failures and communication losses.**

***Index Terms*—Cooperative control, dc microgrid clusters, distributed control, graph theory, tertiary controller.**

NOMENCLATURE

$\mathbf{A}$	Adjacency matrix of the communication graph for the global tertiary controller.
$\mathbf{A}^k$	Adjacency matrix of the communication graph for the local tertiary controller of microgrid k.
F^k	Set of converter agents controlled (pinned) by microgrid agent k.
g_i^k	Pinning gain of converter i in microgrid k.
$\mathbf{G}^k$	Diagonal matrix of pinning gains for microgrid k.
$\mathbf{G}_{\rm c}(s)$	Diagonal PI controller matrix of global tertiary controller.
$i_{{\rm pu},i}^k$	Per-unit current of source i in microgrid k.
$\mathbf{i}_{\rm pu}^k, \mathbf{I}_{\rm pu}^k$	Vector of per-unit currents in microgrid k and its Laplace transform, respectively.
$\mathbf{i}^k, \mathbf{I}^k$	Vector of source currents in microgrid k and its Laplace transform, respectively.
$i_{\rm pu}^k$	Average of per-unit currents in microgrid k.
$\mathbf{i}_{\rm pu}, \mathbf{I}_{\rm pu}$	Global vector of averaged per-unit currents for all microgrids and its Laplace transform, respectively.
$\mathbf{L}$	Laplacian matrix of the communication graph for the global tertiary controller.
$\mathbf{L}^k$	Laplacian matrix of the communication graph for the local tertiary controller of microgrid k.
M	Number of microgrids in the cluster.
S_k	Number of converters in microgrid k.
$v_{\rm ref}$	Global reference voltage (rated voltage) of the overall system.
$\underline{\mathbf{v}}_{\rm ref}, \underline{\mathbf{V}}_{\rm ref}$	Vector of rated voltage of the system and its Laplace transform, respectively.
$v_{\rm ref}^k$	Voltage set point for microgrid k.
$\underline{\mathbf{v}}_{\rm ref}^k, \underline{\mathbf{V}}_{\rm ref}^k$	Vector of voltage set point for microgrid k and its Laplace transform, respectively.
$\mathbf{v}_{\rm ref}, \mathbf{V}_{\rm ref}$	Vector of voltage set points for all microgrids and its Laplace transform, respectively.
$v_{{\rm ref},i}^k$	Local voltage set point for converter i in microgrid k.
$\mathbf{v}_{\rm ref}^k, \mathbf{V}_{\rm ref}^k$	Vector of local voltage set points for all converters in microgrid k and its Laplace transform, respectively.

Manuscript received October 20, 2014; revised February 21, 2015; accepted April 16, 2015. Date of publication April 20, 2015; date of current version September 29, 2015. This work was supported in part by the National Science Foundation under Grant ECCS-1405173 and by the U.S. Office of Naval Research under Grant N00014-14-1-0718. Recommended for publication by Associate Editor T.-F. Wu.

The authors are with the Electrical Engineering Department, University of Texas at Arlington, TX 76019 USA (e-mail: seyedali.moayedi@mavs.uta.edu; davoudi@uta.edu).

Color versions of one or more of the figures in this paper are available online at http://ieeexplore.ieee.org.

Digital Object Identifier 10.1109/TPEL.2015.2424672

I. INTRODUCTION

MICROGRID is a small-scale power system, consisting of generation units, loads, and storage units [1]–[3], that can act independently of the main grid. It has gained significant attention recently [4]–[6], for its desired characteristics such as improved relibility [7]–[10], efficiency [11], [12], stability, and expandability [13]–[15]. Although conventional applications of microgrids utilize inverter-based ac systems, contemporary applications are moving toward a dc microgrid paradigm. This is expected as majority of the emerging renewable energy sources (e.g., solar), storage components (e.g., batteries and ultracapacitors), and loads (e.g., electronics, motor drives, LED lighting, electric vehicle chargers) are inherently dc [12], [16], [17]. Therefore, moving toward a dc distribution paradigm would eliminate unnecessary conversion stages and improve overall efficiency and reliability. In addition, dc microgrids enjoy a simpler control structure and do not deal with inrush currents, frequency synchronization, power quality, etc., which afflict ac microgrids [18], [19].

The hierarchical control system of microgrids includes primary, secondary, and tertiary control levels that act on different timescales [4], [20]–[26]. The primary controllers collectively

balance generations among sources within a microgrid. Voltage drifts/offsets caused by such regulation should be compensated using the secondary controller. Moreover, as shown in [27], the primary controller alone does not have a satisfactory load sharing performance, especially where the transmission line impedances are not negligible. Accordingly, the authors in [19] and [27] propose cooperative primary–secondary control to regulate the output voltages of sources within a microgrid and properly share the load current among them. In the islanded mode of operation, the voltage set point used in the secondary (and primary) control levels is usually the rated voltage of the microgrid. Upon connection to the main grid, or other microgrids, the power transferred to/from the microgrid should be adjusted. This task is assigned to the tertiary controller to adjust the voltage set points for the microgrid and control its power flow.

Microgrids can be connected to each other and form a cluster. Microgrids in a close vicinity might utilize their energy sources differently. Balancing the utilization factors would help reduce the aging of the individual power electronic components and increase their reliability and lifespan [28]–[30]. While connected, the power flow among microgrids may be controlled to balance the utilization factors of their energy sources by adjusting their bus voltages. Tertiary control of dc microgrids is discussed in the literature to control the power flow between the microgrid and the main grid, from economical, optimality, and stability perspectives [31]–[36]. However, controlling the power flow among microgrids within a cluster has not received sufficient attention yet.

Control structures of multiagent systems can be grouped into centralized, decentralized, and distributed categories. In centralized control systems [4], [37], the controller collects the data from all the agents, generates command signals, and sends them back to individual agents. The structure of a centralized control system requires establishment of two-way, high bandwidth communication links between the central controller and every other agent, which reduces system's reliability by exposing a single point-of-failure. In decentralized control systems [10], [38], individual controllers are embedded in the agents, with no communication, and every agent fulfills its own control objective. However, exchange of information, even limited, can help shape the global reference signals and ensure that modules share a common control objective. Thus, the local controllers cannot adequately adapt to the changes in the system-level (global) information and objectives. In distributed control systems [19], [27], [39]–[42], every agent features an embedded controller, which communicates with other agents through a cyber network to discharge the global control objectives. The communication network is sparse, and every agent communicates with a few other agents (neighbors). Compared to a fully connected network, this sparse network helps reduce the communication infrastructure costs and makes it scaleable.

This paper studies a distributed two-level tertiary control system to adjust the voltage set points of individual microgrids and balance the loading among all the sources throughout the cluster. This distributed tertiary control paradigm builds upon the primary–secondary control method by the authors in [19]. The contributions of this paper can be summarized as follows:

1) Using cooperation among microgrid agents, the global tertiary controller generates the voltage set point for each microgrid to proportionally share the load among all microgrids within the cluster.
2) Using cooperation among converter agents, the local tertiary controller propagates the global voltage set point across the converters in a microgrid, so that all of them reach a consensus on their local voltage set points.
3) The local tertiary controller is fully distributed; it shares the communication graph with the distributed secondary controller not to add to the system complexity. Since the voltage set points are not directly sent to all converter agents, reliability concerns due to the presence of a single point-of-failure are avoided.
4) The global tertiary controller is robust against physical (i.e., microgrid disconnection) and cyber (i.e., communication link) failures so long as the remaining communication graph has a spanning tree. It does not need *a priori* knowledge of (or knowledge update for) the number of microgrids (or the converters within each microgrid). Therefore, it provides a plug-and-play capability for participating microgrids.

The remainder of this paper is outlined as follows: Section II explains the preliminary of graph theory and cooperative control. In Section III, the proposed distributed tertiary controller is discussed. Section IV provides the overall dynamic model and shows the efficacy of the proposed controller. The proposed tertiary controller is experimentally verified in Section V. Section VI concludes this paper.

II. Cooperative Control Framework: Intraction on Graphs

Cooperative control offers interaction of control plants in a dynamic multiagent system. Each control agent exchanges data with some other agents on a communication network and processes the data to control its associated system. The communication network is sparse, i.e., each agent communicates with only a few other agents. Graph theory is used for graphical representation of the communication network [30], [43]–[46]. In general, cooperative control problems can be categorized as synchronization and tracking problems [44]. The two types of cooperative control problems, along with the graph theory, are discussed in this section.

A. Graph Theory

A graph is a set of nodes which are connected to each other through a set of edges. An example of a simple (or leaderless) graph is shown in Fig. 1(a). Each edge on the graph shows the communication between two nodes. As seen in Fig. 1, the edges on the graph can be unidirectional or bidirectional. The direction of an edge on the graph represents the information flow direction. If all the edges within a graph are bidirectional, the graph is undirected. Otherwise, it is a directed graph. A

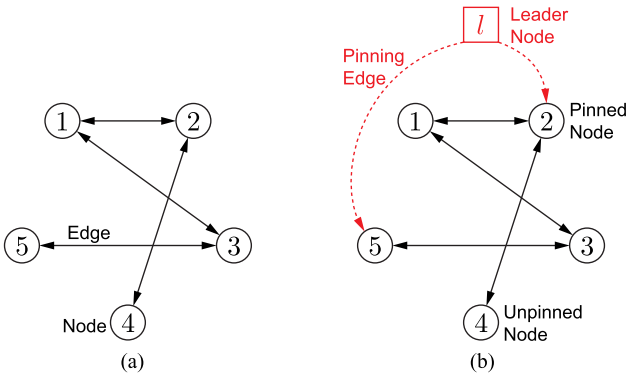

Fig. 1. Graphical representation of a distributed cooperative system: (a) Leaderless graph for a synchronization problem. (b) Pinned graph for a tracking problem.

set of neighbors is defined for each node on the graph, which includes all the nodes which send information to that specific node. This set is represented by N_i for node i on the graph. It is noteworthy that on a directed graph, neighborhood is not necessarily reciprocal. In other words, if node j is a neighbor of node i ($j \in N_i$), node i might not be a neighbor of node j. A nonnegative communication weight is assigned to each edge. This weight is shown by a_{ij} for the edge from node j to node i. In addition, if there is no data transfer from node j to node i, the corresponding weight a_{ij} is zero. Considering N nodes on the graph, the adjacency matrix is defined to carry the communication weights as

$$\mathbf{A} = [a_{ij}] \in \mathbb{R}^{N\times N}. \tag{1}$$

The diagonal in-degree matrix, $\mathbf{D} = \text{diag}\{d_i\} \in \mathbb{R}^{N\times N}$, carries the in-degree of each node, which is defined as the sum of communication weights from neighbors of that node

$$d_i = \sum_{j\in N_i} a_{ij} = \sum_{j=1}^{N} a_{ij}. \tag{2}$$

Then, the Laplacian matrix is defined as $\mathbf{L} \triangleq \mathbf{D} - \mathbf{A}$. Since the row-sums of $\mathbf{D}$ and $\mathbf{A}$ are equal, the row sums of $\mathbf{L}$ are all zero. Accordingly, one can write

$$\mathbf{L}\begin{bmatrix}1 & \dots & 1\end{bmatrix}^{\mathrm{T}} = \mathbf{0}. \tag{3}$$

Equivalently, the vector $\underline{\mathbf{1}} = \begin{bmatrix}1 & \dots & 1\end{bmatrix}^{\mathrm{T}}$ is a right eigenvector of $\mathbf{L}$ with $\lambda_1 = 0$ as the corresponding eigenvalue. Similar to the in-degree, the out-degree of node i is the sum of communication weights from node i to other nodes on the graph. If the in-degree is equal to the out-degree for every node, the associated Laplacian matrix is said to be balanced. A graph is said to have a *spanning tree* upon reachability of all nodes in a graph from at least one single (root) node. A graph is *strongly connected* if there is a path between every two nodes, i.e., there exists a spanning tree where all nodes are root nodes. If a graph has a spanning tree, the Laplacian matrix eigenvalue $\lambda_1 = 0$ is a simple eigenvalue [44], [45]. Accordingly, $\mathbf{L}$ has rank of $N-1$ and $\underline{\mathbf{1}} \in \text{Null}(\mathbf{L})$. Therefore, the only solution to $\mathbf{Lx} = \mathbf{0}$ can be written as $\mathbf{x} = c\underline{\mathbf{1}}$, where c is a constant.

A leader node can be added to a strongly connected graph and be connected to at least one node(s) by unidirectional edge(s). The nodes connected to the leader node and the corresponding connecting edge are called *pinned* (controlled) nodes and pinning edge, respectively. The resulting graph is also called the pinned graph. An example of a pinned graph is shown in Fig. 1(b), where nodes 2 and 5 are pinned nodes. As shown, the direction of the pinning edge implies the unidirectional information flow from the leader node to the pinned nodes. A nonnegative gain is assigned to each pinning edge, which is shown by g_i for the pinning gain from the leader node to node i. The pinning gain is zero for an unpinned node. The pinning matrix is defined to carry all the pinning gains of the graph

$$\mathbf{G} = \text{diag}\{g_i\} \in \mathbb{R}^{N\times N}. \tag{4}$$

Although the Laplacian matrix of a leaderless graph is singular, when added to the pinning gain matrix, the resulted matrix $\mathbf{L}+\mathbf{G}$ is invertible. In addition, all the eigenvalues of $\mathbf{L}+\mathbf{G}$ have positive real parts [44].

B. Synchronization Problem

In a cooperative synchronization problem, every agent has a specific local variable (or a vector of variables), which is desired to be synchronized with that of other agents. This is also called *consensus* in the literature [19], [45]–[48]. A leaderless graph can be used to model a cooperative synchronization problem, where every node represents a control agent and every edge shows a communication link. The synchronization problem can be stated as achieving consensus in all elements of the global vector $\mathbf{x} = \begin{bmatrix}x_1 & \dots & x_N\end{bmatrix}^{\mathrm{T}}$, where x_i belongs to agent i. To reach consensus, the graph should contain at least one spanning tree. Then, the distributed control agents cooperate to hold $\mathbf{Lx} = \mathbf{0}$ at the steady state. Therefore, the only feasible steady-state value of $\mathbf{x}$ is $\mathbf{x} = c\underline{\mathbf{1}}$, which guarantees the consensus for the elements of vector $\mathbf{x}$. It should be noted, in a synchronization problem, the value at which the variables reach consensus, i.e., c in $\mathbf{x} = c\underline{\mathbf{1}}$, is not a control objective and is dictated by the plant parameters.

C. Tracking Problem

Similar to a synchronization problem, the goal of a cooperative tracking problem is to have consensus for the agent variables. However, unlike the synchronization problem, the consensus value is a control objective usually provided by the *leader*. One can state the tracking problem as $\mathbf{x} = \underline{\mathbf{1}}x_{\text{ref}}$, where x_{ref} is the reference value determined by the leader. The leader is connected to a limited number of agents. A pinned graph is used to model the tracking problem [see Fig. 1(b)] . To reach consensus at the reference value, the graph should contain at least one pinned root node. Then, the control agents cooperate to hold

$$\dot{\mathbf{x}} = -(\mathbf{L}+\mathbf{G})(\mathbf{x} - \underline{\mathbf{1}}x_{\text{ref}}) \tag{5}$$

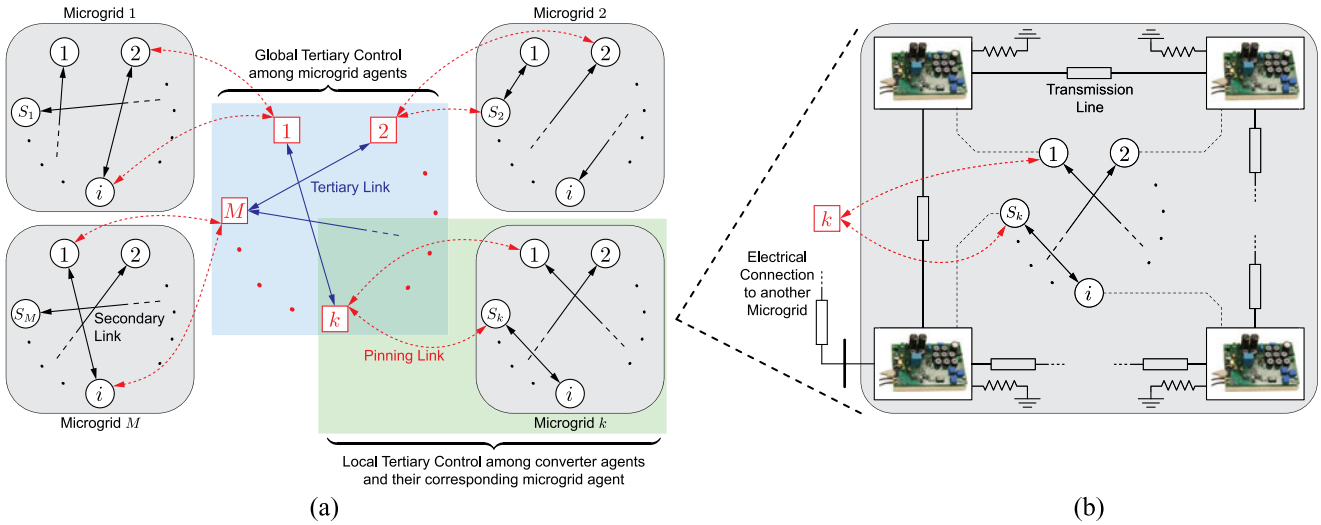

Fig. 2. Cyber and electrical connection layouts in a cluster of microgrids: (a) Cooperation of control agents on graphs for global and local tertiary controllers. Microgrid agents are shown with highlighted squares and converter agents are shown with circles (b) Physical layout of a dc microgrid, including energy sources, loads, and transmission lines.

at the steady state. Since all eigenvalues of $\mathbf{L}+\mathbf{G}$ have positive real values, equation (5) results in the desired tracking performance at the steady state. It is noteworthy that the reference value can also have dynamics. However, to have acceptable tracking performance for all agents, the dynamics of the tracking equation (5) should be much faster than those of the reference.

III. Distributed Tertiary Control

The proposed distributed tertiary control operates at two levels. As shown in Fig. 2, every microgrid has a dedicated control agent, which is represented by a highlighted square node. A cyber network connects microgrid agents, which are mapped into the tertiary graph, where tertiary links represent data exchange among microgrid agents. As seen in Fig. 2(b), each microgrid has also electrical connection to other microgrids through transmission lines, where the electrical network among microgrids may differ from the cyber network among corresponding microgrid agents. Cooperation among microgrid agents, through the tertiary graph, develops the higher level tertiary control, i.e., global tertiary control, where the set points for each microgrid are generated. In addition, converter agents inside each microgrid are represented by circle nodes, which are connected through secondary links in a cyber network. As seen in Fig. 2(b), this cyber network may differ from the electrical network among the sources within the microgrid, where dispatchable sources (only the controllable dc–dc converters are shown) are connected to each other through transmission lines. Some converter agents in each microgrid are pinned by their corresponding microgrid agent. The lower level tertiary controller, i.e., the local tertiary controller, benefits from cooperation of converter agents and the leadership of the microgrid agents to propagate the generated voltage set points inside each microgrid. As it will be described later, the global and local tertiary controllers cooperate to balance the source currents across the microgrids clusters.

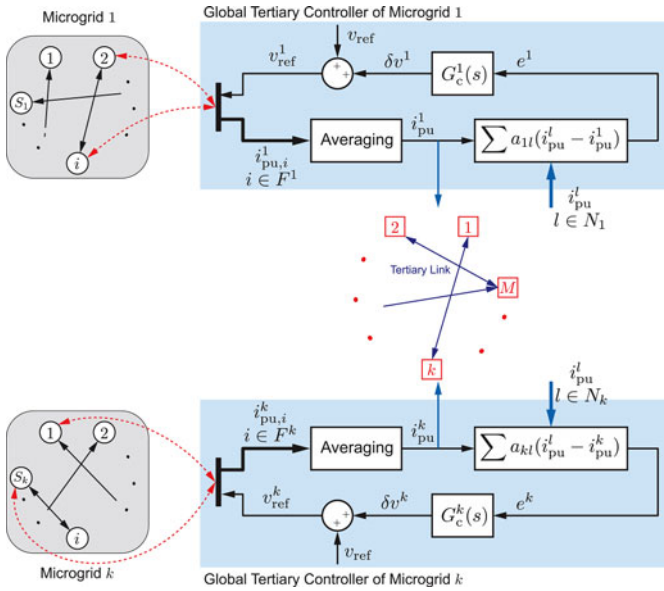

Fig. 3. Block diagram of the distributed global tertiary controller for a number of microgrid agents.

A. Global Tertiary Controller

Global tertiary controllers cooperate to adjust the voltage set point for each microgrid, e.g., $v^k_{\rm ref}$ for microgrid k. This network is represented by the tertiary graph shown in Fig. 3, where the microgrid agents are represented by highlighted square nodes. Each microgrid agent should know its local load $i^k_{\rm pu}$ which is the average of per-unit currents of its sources $i^k_{{\rm pu},i}$. The per-unit term here refers to the current provided by the converter divided by its rated current. This terminology of the per-unit current is used here to represent loading percentage of each converter. The microgrid agents are connected on a sparse communication network and exchange the data of their local load $i^k_{\rm pu}$. As shown in

Fig. 3, pinning links connect each microgrid agent to a number of converter agents (pinned converter agents), which can be used to transfer the data of per-unit currents to the microgrid agents. The secondary controller is supposed to balance the per-unit currents of all the sources within each microgrid. Accordingly, the per-unit current of each converter $i^k_{\mathrm{pu},i}$ can represent the average per-unit current of all sources in the corresponding microgrid at the steady state i^k_{pu}. Although, to increase reliability, the microgrid agent may receive data from more than one converter agent. The microgrid agent can then have the average per-unit current of its sources

$$i^k_{\mathrm{pu}} = \frac{1}{|F^k|}\sum_{i\in F^k} i^k_{\mathrm{pu},i} \tag{6}$$

where F^k is the set of pinned converter agents in microgrid k and $|F^k|$ is the cardinality of F^k.

The tertiary graph, containing M microgrid agents, has an adjacency matrix $\mathbf{A} = [a_{kl}] \in \mathbb{R}^{M\times M}$. Once microgrid agent k knows its own local load, it compares that with those of its neighbors, i.e., other microgrid agents, which send data to microgrid agent k through tertiary links. The comparison is performed through a *local voting protocol*

$$e^k = \sum_{l\in N_k} a_{kl}\left(i^l_{\mathrm{pu}} - i^k_{\mathrm{pu}}\right) \tag{7}$$

where N_k is the set of neighbors of microgrid agent k on the tertiary communication graph. The error term e^k can be written as the difference of the local load in microgrid k and the weighted average of the load of its neighbors

$$\begin{aligned} e^k &= -i^k_{\mathrm{pu}}\sum_{l\in N_k} a_{kl} + \sum_{l\in N_k} a_{kl} i^l_{\mathrm{pu}} \\ &= -d_k i^k_{\mathrm{pu}} + \sum_{l\in N_k} a_{kl} i^l_{\mathrm{pu}} \\ &= d_k\left(-i^k_{\mathrm{pu}} + \sum_{l\in N_k}\frac{a_{kl}}{d_k} i^l_{\mathrm{pu}}\right). \end{aligned} \tag{8}$$

This error term is then processed through a PI controller to generate the voltage correction term δv^k. As shown in Fig. 3, this voltage correction term is added to the global reference voltage, v_{ref}, which is the rated voltage of the microgrid cluster system

$$v^k_{\mathrm{ref}} = v_{\mathrm{ref}} + \delta v^k \tag{9}$$

where v^k_{ref} is the local voltage set point for microgrid k. When microgrid k has less local load than its neighbors, the error term e^k becomes positive, which increases the output of PI controller, δv^k and, consequently, raises the local voltage set point v^k_{ref}. Accordingly, the local voltage set points of the converter agents in microgrid k escalate through the local tertiary control system, which result in compensation for the low source currents in microgrid k.

B. Local Tertiary Controller

Once the local voltage set points of all microgrids v^k_{ref} are generated, they must be sent to all converter agents within each microgrid. A straight forward approach is to directly transmit voltage set points toward all converter agents. However, any single communication failure hinders system functionality. Alternatively, a distributed approach is proposed to improve system reliability without adding to its complexity. The secondary controller in microgrid k features a communication network between S_k converters, which is modeled by a graph with adjacency matrix $\mathbf{A}^k = [a^k_{ij}] \in \mathbb{R}^{S_k\times S_k}$. The proposed local tertiary controller, exploits the existing communication infrastructure, used by the secondary controllers, to propagate the generated voltage set points across each microgrid. To this end, some converter agents will be pinned by their associated microgrid agent to receive the voltage set point directly. The pinning links are basically unidirectional links, used to transmit the data from the leader (microgrid agent) to the pinned converter agents. However, the existing communication link can be used as a bidirectional link, which also transmits the local load data from the pinned node to the leader node in the global tertiary controller. A local voting protocol then updates the voltage set point for both pinned and unpinned converter agents

$$\dot{v}^k_{\mathrm{ref},i} = \sum_{j\in N^k_i} a^k_{ij}\left(v^k_{\mathrm{ref},j} - v^k_{\mathrm{ref},i}\right) + g^k_i\left(v^k_{\mathrm{ref}} - v^k_{\mathrm{ref},i}\right) \tag{10}$$

where $v^k_{\mathrm{ref},i}$ and g^k_i are the local set point and pinning gain of converter agent i in microgrid k, respectively. The pinning gain g^k_i is positive if the converter agent i is pinned by the microgrid agent k, and is zero otherwise.

Fig. 4 presents the block diagram of the local tertiary control system in microgrid k. As seen in Fig. 4, the pinned converter agents update their voltage set points based on data received from the microgrid agent and its neighbor converter agents. On the other hand, unpinned converter agents update their voltage set point based on received data only from their neighbors, which can be pinned or unpinned converter agents. One can say that two terms affect the change rate in the voltage set point of a converter agent $v^k_{\mathrm{ref},i}$: 1) Its deviation from the weighted

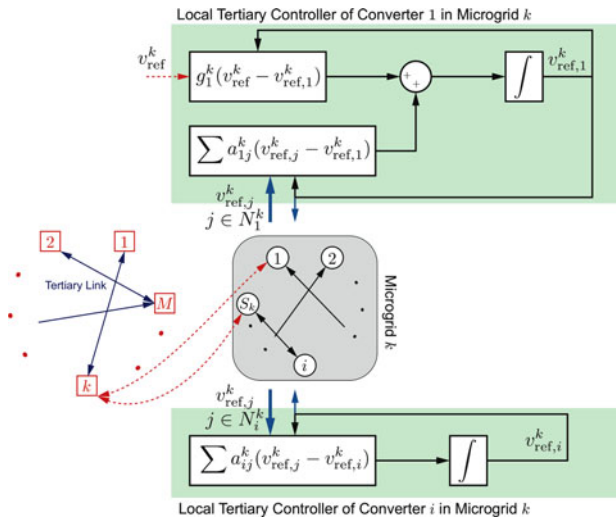

Fig. 4. Block diagram of the distributed local tertiary controller for pinned and unpinned converter agents inside microgrid k.

average of that of its neighbors; 2) its deviation from the set point of the microgrid agent $v_{\rm ref}^k$ (for pinned converter agents only).

It will be shown in Section IV-E that if the secondary graph is strongly connected and has, at least, one pinned node, the voltage set points of all converter agents in each microgrid $v_{{\rm ref},i}^k$ become equal to that of its corresponding microgrid agent $v_{\rm ref}^k$ at the steady state. In other words, the voltage set point generated at the global tertiary controller is propagated across all converter agents in the microgrid.

IV. Dynamic Model Development

Dynamic models of both global and local tertiary controllers are extracted. These models can then be combined with the microgrid physical model to analyze the system-level performance. The steady-state analysis verifies the controller performance in achieving the load sharing goals.

A. Global Tertiary Modeling

The modeling of global tertiary controller can be started by writing (6) in a matrix format. Let $\mathbf{G}_{\rm N}^k \in \mathbb{R}^{S_k \times S_k} = {\rm sign}\{\mathbf{G}^k\}$. Accordingly, the number of converter agents pinned by the microgrid agent k can be written as

$$|F^k| = \underline{\mathbf{1}}^{\rm T} \mathbf{G}_{\rm N}^k \underline{\mathbf{1}}. \tag{11}$$

In addition, the sum of per-unit currents of pinned converters in microgrid k can be written in the matrix format

$$\sum_{i \in F^k} i_{{\rm pu},i}^k = \underline{\mathbf{1}}^{\rm T} \mathbf{G}_{\rm N}^k \mathbf{i}_{\rm pu}^k \tag{12}$$

where $\mathbf{i}_{\rm pu}^k = \left[i_{{\rm pu},1}^k \ \cdots \ i_{{\rm pu},S_k}^k \right]^{\rm T} \in \mathbb{R}^{S_k \times 1}$. Accordingly, (6) can be written as

$$i_{\rm pu}^k = \left(\underline{\mathbf{1}}^{\rm T} \mathbf{G}_{\rm N}^k \underline{\mathbf{1}} \right)^{-1} \underline{\mathbf{1}}^{\rm T} \mathbf{G}_{\rm N}^k \mathbf{i}_{\rm pu}^k \tag{13}$$

where $\underline{\mathbf{1}} \in \mathbb{R}^{S_k \times 1}$. Then, the vector containing the local loads of all microgrids can be written as

$$\mathbf{i}_{\rm pu} = \begin{bmatrix} \left(\underline{\mathbf{1}}^{\rm T} \mathbf{G}_{\rm N}^1 \underline{\mathbf{1}} \right)^{-1} \underline{\mathbf{1}}^{\rm T} \mathbf{G}_{\rm N}^1 \mathbf{i}_{\rm pu}^1 \\ \vdots \\ \left(\underline{\mathbf{1}}^{\rm T} \mathbf{G}_{\rm N}^M \underline{\mathbf{1}} \right)^{-1} \underline{\mathbf{1}}^{\rm T} \mathbf{G}_{\rm N}^M \mathbf{i}_{\rm pu}^M \end{bmatrix}. \tag{14}$$

One can write (14) in the frequency domain

$$\mathbf{I}_{\rm pu} = \begin{bmatrix} \left(\underline{\mathbf{1}}^{\rm T} \mathbf{G}_{\rm N}^1 \underline{\mathbf{1}} \right)^{-1} \underline{\mathbf{1}}^{\rm T} \mathbf{G}_{\rm N}^1 \mathbf{I}_{\rm pu}^1 \\ \vdots \\ \left(\underline{\mathbf{1}}^{\rm T} \mathbf{G}_{\rm N}^M \underline{\mathbf{1}} \right)^{-1} \underline{\mathbf{1}}^{\rm T} \mathbf{G}_{\rm N}^M \mathbf{I}_{\rm pu}^M \end{bmatrix} \tag{15}$$

where $\mathbf{I}_{\rm pu}$ and $\mathbf{I}_{\rm pu}^k$ are the Laplace transforms of $\mathbf{i}_{\rm pu}$ and $\mathbf{i}_{\rm pu}^k$, respectively.

The matrix format of (7) can be written as

$$\mathbf{e} = -\mathbf{L} \mathbf{i}_{\rm pu} \tag{16}$$

where $\mathbf{e} = \left[e^1 \ \cdots \ e^M \right]^{\rm T} \in \mathbb{R}^{M \times 1}$ and $\mathbf{L}$ is the Laplacian matrix of tertiary graph. In the frequency domain

$$\mathbf{E} = -\mathbf{L} \mathbf{I}_{\rm pu} \tag{17}$$

where $\mathbf{E}$ is the Laplace transform of $\mathbf{e}$. Similarly, (9) can be written in the matrix format

$$\begin{aligned} \mathbf{v}_{\rm ref} &= \underline{\mathbf{1}} v_{\rm ref} + \delta \mathbf{v} \\ &= \underline{\mathbf{v}}_{\rm ref} + \delta \mathbf{v} \end{aligned} \tag{18}$$

where $\mathbf{v}_{\rm ref} = \left[v_{\rm ref}^1 \ \cdots \ v_{\rm ref}^M \right]^{\rm T}$, $\delta \mathbf{v} = \left[\delta v^1 \ \cdots \ \delta v^M \right]^{\rm T}$, and $\underline{\mathbf{v}}_{\rm ref} = \left[v_{\rm ref} \ \cdots \ v_{\rm ref} \right]^{\rm T} \in \mathbb{R}^{M \times 1}$. One can write (18) in the frequency domain

$$\begin{aligned} \mathbf{V}_{\rm ref} &= \underline{\mathbf{V}}_{\rm ref} + \Delta \mathbf{V} \\ &= \underline{\mathbf{V}}_{\rm ref} - \mathbf{G}_{\rm c} \mathbf{L} \mathbf{I}_{\rm pu} \end{aligned} \tag{19}$$

where $\mathbf{V}_{\rm ref}$, $\underline{\mathbf{V}}_{\rm ref}$, and $\Delta \mathbf{V}$ are the Laplace transforms of $\mathbf{v}_{\rm ref}$, $\underline{\mathbf{v}}_{\rm ref}$, and $\delta \mathbf{v}$, respectively. $\mathbf{G}_{\rm c} = {\rm diag}\{G_{\rm c}^k\} \in \mathbb{R}^{M \times M}$ is the PI controller matrix used in the global tertiary system. One can substitute $\mathbf{I}_{\rm pu}$ from (15) to obtain

$$\mathbf{V}_{\rm ref} = \underline{\mathbf{V}}_{\rm ref} - \mathbf{G}_{\rm c} \mathbf{L} \begin{bmatrix} \left(\underline{\mathbf{1}}^{\rm T} \mathbf{G}_{\rm N}^1 \underline{\mathbf{1}} \right)^{-1} \underline{\mathbf{1}}^{\rm T} \mathbf{G}_{\rm N}^1 \mathbf{I}_{\rm pu}^1 \\ \vdots \\ \left(\underline{\mathbf{1}}^{\rm T} \mathbf{G}_{\rm N}^M \underline{\mathbf{1}} \right)^{-1} \underline{\mathbf{1}}^{\rm T} \mathbf{G}_{\rm N}^M \mathbf{I}_{\rm pu}^M \end{bmatrix}. \tag{20}$$

One can define $\mathbf{I}_{\rm rated}^k \triangleq {\rm diag}\{I_{{\rm rated},i}^k\} \in \mathbb{R}^{S_k \times S_k}$, where $I_{{\rm rated},i}^k$ is the rated current of converter i in microgrid k. Accordingly, $\mathbf{I}_{\rm pu}^k = {\mathbf{I}_{\rm rated}^k}^{-1} \mathbf{I}^k$, where $\mathbf{I}^k$ is the Laplace transform of $\mathbf{i}^k \in \mathbb{R}^{S_k \times 1}$, the vector of currents in microgrid k. Therefore, (20) can be written as

$$\mathbf{V}_{\rm ref} = \underline{\mathbf{V}}_{\rm ref} - \mathbf{G}_{\rm c} \mathbf{L} \begin{bmatrix} \left(\underline{\mathbf{1}}^{\rm T} \mathbf{G}_{\rm N}^1 \underline{\mathbf{1}} \right)^{-1} \underline{\mathbf{1}}^{\rm T} \mathbf{G}_{\rm N}^1 {\mathbf{I}_{\rm rated}^1}^{-1} \mathbf{I}^1 \\ \vdots \\ \left(\underline{\mathbf{1}}^{\rm T} \mathbf{G}_{\rm N}^M \underline{\mathbf{1}} \right)^{-1} \underline{\mathbf{1}}^{\rm T} \mathbf{G}_{\rm N}^M {\mathbf{I}_{\rm rated}^M}^{-1} \mathbf{I}^M \end{bmatrix}. \tag{21}$$

Defining $\mathbf{C}^k \triangleq \left(\underline{\mathbf{1}}^{\rm T} \mathbf{G}_{\rm N}^k \underline{\mathbf{1}} \right)^{-1} \underline{\mathbf{1}}^{\rm T} \mathbf{G}_{\rm N}^k {\mathbf{I}_{\rm rated}^k}^{-1} \in \mathbb{R}^{1 \times S_k}$, one can write (21) as

$$\mathbf{V}_{\rm ref} = \underline{\mathbf{V}}_{\rm ref} - \mathbf{G}_{\rm c} \mathbf{L} \begin{bmatrix} \mathbf{C}^1 \mathbf{I}^1 \\ \vdots \\ \mathbf{C}^M \mathbf{I}^M \end{bmatrix} \tag{22}$$

which concludes the global modeling of the tertiary controller.

B. Local Tertiary Modeling

In order to model the local tertiary controller, (10) can be written in a matrix format. One can define $\mathbf{v}_{\rm ref}^k = \left[v_{{\rm ref},1}^k \ \cdots \ v_{{\rm ref},S_k}^k \right]^{\rm T}$ and $\underline{\mathbf{v}}_{\rm ref}^k = \left[v_{\rm ref}^k \ \cdots \ v_{\rm ref}^k \right]^{\rm T} \in \mathbb{R}^{S_k \times 1}$. Accordingly, (10) can be written in the matrix format as

$$\begin{aligned} \dot{\mathbf{v}}_{\rm ref}^k &= -\left(\mathbf{L}^k + \mathbf{G}^k \right) \left(\mathbf{v}_{\rm ref}^k - \underline{\mathbf{1}} v_{\rm ref}^k \right) \\ &= -\left(\mathbf{L}^k + \mathbf{G}^k \right) \left(\mathbf{v}_{\rm ref}^k - \underline{\mathbf{v}}_{\rm ref}^k \right) \end{aligned} \tag{23}$$

where $\mathbf{L}^k$ is the Laplacian matrix of the communication graph for the secondary control of microgrid k and $\mathbf{G}^k = \text{diag}\{g_i^k\} \in \mathbb{R}^{S_k \times S_k}$. One can define $\mathbf{V}_{\text{ref}}^k$ and $\underline{\mathbf{V}}_{\text{ref}}^k$ as the Laplace transforms of $\mathbf{v}_{\text{ref}}^k$ and $\underline{\mathbf{v}}_{\text{ref}}^k$, respectively. Accordingly, (23) can be written in the Laplace domain as

$$s\mathbf{V}_{\text{ref}}^k - \mathbf{v}_{\text{ref}}^k(0) = -\left(\mathbf{L}^k + \mathbf{G}^k\right)\left(\mathbf{V}_{\text{ref}}^k - \underline{\mathbf{V}}_{\text{ref}}^k\right). \tag{24}$$

Assuming zero initial condition for the local voltage set points of each converter at microgrid k, one can write (24) as

$$s\mathbf{V}_{\text{ref}}^k = -\left(\mathbf{L}^k + \mathbf{G}^k\right)\left(\mathbf{V}_{\text{ref}}^k - \underline{\mathbf{V}}_{\text{ref}}^k\right). \tag{25}$$

Equivalently

$$\begin{aligned}\mathbf{V}_{\text{ref}}^k &= \left(s\mathbf{I}_{N_k} + \mathbf{L}^k + \mathbf{G}^k\right)^{-1}\left(\mathbf{L}^k + \mathbf{G}^k\right)\underline{\mathbf{V}}_{\text{ref}}^k \\ &= \mathbf{T}^k\underline{\mathbf{V}}_{\text{ref}}^k\end{aligned} \tag{26}$$

where $\mathbf{T}^k$ is the transfer function of the local tertiary controller for microgrid k.

C. System-Level Modeling

The system-level model combines the global and local tertiary control models, along with the physical microgrid model, which has the secondary and primary controllers in effect. In order to combine the global and local tertiary controllers, $\underline{\mathbf{V}}_{\text{ref}}^k$ can be obtained from $\mathbf{V}_{\text{ref}}$ by

$$\underline{\mathbf{V}}_{\text{ref}}^k = \mathbf{U}^k\mathbf{V}_{\text{ref}} \tag{27}$$

where $\mathbf{U}^k \in \mathbb{R}^{S_k \times M}$ is a matrix with all zero elements, except for the column k, whose entries are all 1. Then, substituting $\underline{\mathbf{V}}_{\text{ref}}^k$ from (27) into (26), one can write

$$\mathbf{V}_{\text{ref}}^k = \mathbf{T}^k\mathbf{U}^k\mathbf{V}_{\text{ref}} \tag{28}$$

which can be combined with the global tertiary model.

One can define $\mathbf{V}^k$ as the Laplace transform of $\mathbf{v}^k = \left[v_1^k \ \ldots \ v_{S_k}^k\right]^{\text{T}} \in \mathbb{R}^{S_k \times 1}$, the voltage vector in microgrid k. The transfer functions from the reference voltage to the output voltage and current vectors for a microgrid, with distributed secondary and primary controllers, can be written as

$$\begin{cases}\mathbf{V}^k = \mathbf{T}_V^k\mathbf{V}_{\text{ref}}^k \\ \mathbf{I}^k = \mathbf{T}_I^k\mathbf{V}_{\text{ref}}^k\end{cases} \tag{29}$$

where $\mathbf{T}_V^k$ and $\mathbf{T}_I^k \in \mathbb{R}^{S_k \times S_k}$ are the voltage and current transfer functions of microgrid k, respectively. As shown in [19], the transfer functions $\mathbf{T}_V^k$ and $\mathbf{T}_I^k$ depend on microgrid dynamics, as well as primary and secondary controllers, defined in a simplified expression as

$$\begin{cases}\mathbf{T}_V^k = \left(\mathbf{G}_c^{k\,-1} + \mathbf{H}^k\mathbf{Q}_{S_k} + c^k\mathbf{K}^k\mathbf{L}^k{\mathbf{I}_{\text{rated}}^k}^{-1}\mathbf{Y}_{\text{bus}}^k\right)^{-1} \\ \qquad \times \left(\mathbf{I}_{S_k} + \mathbf{H}^k\right) \\ \mathbf{T}_I^k = \mathbf{Y}_{\text{bus}}^k\mathbf{T}_V^k\end{cases} \tag{30}$$

where $\mathbf{G}_c^k$, $\mathbf{H}^k$, and $\mathbf{K}^k \in \mathbb{R}^{S_k \times S_k}$ are the diagonal transfer function matrices of individual sources, voltage controllers, and current controllers in microgrid k, respectively. c^k is the coupling gain between the voltage and current controllers. $\mathbf{Q}_{S_k} \in \mathbb{R}^{S_k \times S_k}$ is a matrix with all elements equal to ${}^1/_{S_k}$ and $\mathbf{Y}_{\text{bus}}^k$ is the admittance matrix of microgrid k. Using (26) and (29), the dynamics of each individual microgrid can be assessed

$$\begin{cases}\mathbf{V}^k = \mathbf{T}_V^k\mathbf{T}^k\underline{\mathbf{V}}_{\text{ref}}^k = \mathbf{T}_V^k\mathbf{T}^k\underline{\mathbf{1}}V_{\text{ref}}^k = \mathbf{H}_V^kV_{\text{ref}}^k \\ \mathbf{I}^k = \mathbf{T}_I^k\mathbf{T}^k\underline{\mathbf{V}}_{\text{ref}}^k = \mathbf{T}_I^k\mathbf{T}^k\underline{\mathbf{1}}V_{\text{ref}}^k = \mathbf{H}_I^kV_{\text{ref}}^k\end{cases} \tag{31}$$

where $\mathbf{H}_V^k$ and $\mathbf{H}_I^k$ are $S_k \times 1$ matrices. Using (31), a detailed study of microgrid dynamics is performed on a typical microgrid in Section V-B. It is noteworthy that (30) is valid if the system dynamics, including the primary and secondary controllers, are much faster than those of the tertiary controller. One can substitute $\mathbf{V}_{\text{ref}}^k$ in (30) with (28) to obtain

$$\begin{cases}\mathbf{V}^k = \mathbf{T}_V^k\mathbf{T}^k\mathbf{U}^k\mathbf{V}_{\text{ref}} \\ \mathbf{I}^k = \mathbf{T}_I^k\mathbf{T}^k\mathbf{U}^k\mathbf{V}_{\text{ref}}.\end{cases} \tag{32}$$

Finally, $\mathbf{V}_{\text{ref}}$ can be substituted from (22) to complete the model. Fig. 5 shows the complete block diagram of the microgrid clusters system. In order to find the global transfer function, one can define $\mathbf{B}^k \triangleq \mathbf{T}_I^k\mathbf{T}^k\mathbf{U}^k$, and $\mathbf{D}^k \triangleq \frac{1}{N_k}{\mathbf{U}^k}^{\text{T}}\underline{\mathbf{1}}\mathbf{C}^k$. Then, the block diagram of Fig. 5 can be simplified into the block diagram shown in Fig. 6. Accordingly, one can write

$$\mathbf{V}_{\text{ref}} = \underline{\mathbf{V}}_{\text{ref}} - \mathbf{G}_{\text{c}}\mathbf{L}\sum_{k=1}^{M}\mathbf{D}^k\mathbf{B}^k\mathbf{V}_{\text{ref}}. \tag{33}$$

Then, $\underline{\mathbf{V}}_{\text{ref}}$ can be written in terms of the system input, $\underline{\mathbf{V}}_{\text{ref}}$

$$\mathbf{V}_{\text{ref}} = \left(\mathbf{I}_M + \mathbf{G}_{\text{c}}\mathbf{L}\sum_{k=1}^{M}\mathbf{D}^k\mathbf{B}^k\right)^{-1}\underline{\mathbf{V}}_{\text{ref}}. \tag{34}$$

Finally, the transfer function from $\underline{\mathbf{V}}_{\text{ref}}$ to the current vector $\mathbf{I}^k$ can be written as

$$\mathbf{I}^k = \mathbf{B}^k\left(\mathbf{I}_M + \mathbf{G}_{\text{c}}\mathbf{L}\sum_{k=1}^{M}\mathbf{D}^k\mathbf{B}^k\right)^{-1}\underline{\mathbf{V}}_{\text{ref}} \tag{35}$$

which concludes the system-level modeling of a microgrid cluster with the proposed controller in effect.

D. Design Guidelines

The design guidelines for the primary and secondary controllers are discussed in detail in [19]. Accordingly, it is assumed that the primary and secondary controllers have satisfactory dynamic and steady-state behaviors. Therefore, the only design parameters are pinning matrices $\mathbf{G}^k$, global Laplacian matrix $\mathbf{L}$, and global tertiary controller matrix $\mathbf{G}_{\text{c}}(s)$. In other words, pinning converter agents and pinning weights, communication structure and link weights for the tertiary graph, and PI controllers at each microgrid agent should be determined. Dynamics of secondary and primary controllers are neglected compared to that of the tertiary controller. Accordingly, the design parameters should provide slow enough dynamics at the tertiary control level. In addition, the parameters may be chosen such that the system has an asymptotically stable dynamic response, i.e., the poles of the transfer functions in (34) are placed in the open left hand plane (OLHP). It should be noted that since all poles of $\mathbf{T}_I^k$ and $\mathbf{T}^k$ are in the OLHP, the poles of $\mathbf{B}^k$ are also stable.

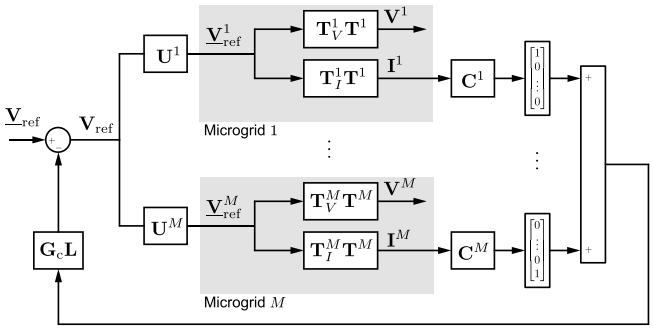

Fig. 5. Global block diagram of the microgrid clusters system.

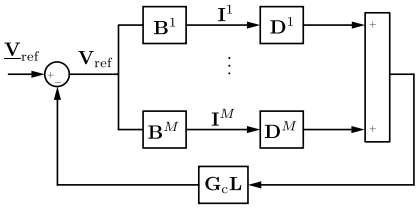

Fig. 6. Simplified block diagram of the microgrid clusters system.

Accordingly, the stability of transfer function in (34) will result in the stability of (35) for all k.

E. Steady-State Analysis

To verify the controller performance in steady state, one should conduct: 1) steady-state analysis of the global tertiary controller, which shows the performance of the load sharing among microgrids; and 2) steady-state analysis of the local tertiary controller, which shows the propagation of the voltage set point for each microgrid v_{ref}^{k} across all corresponding converter agents.

The global tertiary control aims to match the per-unit currents of all sources across the whole cluster, i.e.,

$$i_{\text{pu},i}^{k,\text{ss}} = i_{\text{pu},j}^{l,\text{ss}} \qquad \forall i,j,k,l \tag{36}$$

where x^{ss} is the steady-state value of variable x. Secondary controllers are assumed to be asymptotically stable and balance the load among the sources across each individual microgrid at the steady state. Accordingly, one can write (36) as

$$\mathbf{i}_{\text{pu}}^{\text{ss}} = \underline{\mathbf{1}} i_{\text{pu}}^{k,\text{ss}} \qquad \forall k. \tag{37}$$

The system is assumed to be asymptotically stable. Accordingly, the transfer function from $\underline{\mathbf{V}}_{\text{ref}}$ to $\mathbf{V}_{\text{ref}}$ in (34) has all poles in the OLHP. Therefore, the elements of the vector $\mathbf{v}_{\text{ref}}(t)$ will eventually reach a steady value. Since the tertiary controller matrix $\mathbf{G}_{\text{c}}(s)$ has PI controllers on its diagonal, and its output is constant at the steady state, the integrator part implies that the input of the controller $\mathbf{e}$ must be zero at the steady state, i.e.,

$$\mathbf{e}^{\text{ss}} = \mathbf{0}. \tag{38}$$

Equation (16) can be written in the steady state as

$$\mathbf{e}^{\text{ss}} = -\mathbf{L}\mathbf{i}_{\text{pu}}^{\text{ss}} = \mathbf{0}. \tag{39}$$

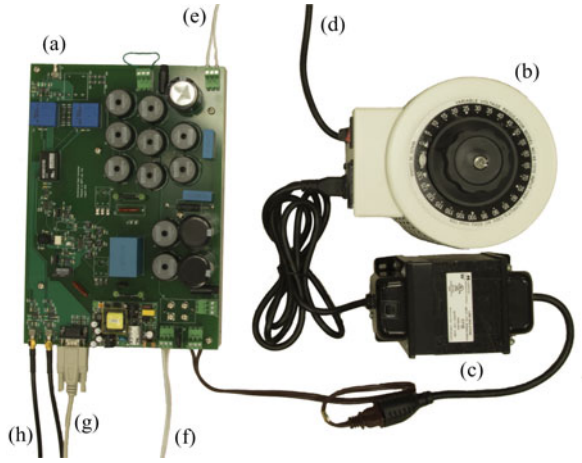

Fig. 7. Energy source in the experimental dc microgrid setup: (a) buck converter, (b) autotransformer, (c) isolation transformer, (d) ac input (power), (e) dc output, (f) ac input (control), (g) control signals, (h) measurement signals.

On the other hand, tertiary communication graph is be designed to have a spanning tree. Therefore, the only answer to $\mathbf{L}\mathbf{i}_{\text{pu}}^{\text{ss}} = \mathbf{0}$ is $\mathbf{i}_{\text{pu}}^{\text{ss}} = c\underline{\mathbf{1}}$, which validates (37) and verifies the desired performance of the load sharing at the steady state.

The local tertiary control propagates the voltage set point of each microgrid across all of its converter agents, i.e.,

$$v_{\text{ref},i}^{k,\text{ss}} = v_{\text{ref}}^{k,\text{ss}} \qquad \forall k,i \tag{40}$$

which can be written in the vector format as

$$\mathbf{v}_{\text{ref}}^{k,\text{ss}} = \underline{\mathbf{v}}_{\text{ref}}^{k,\text{ss}} \qquad \forall k. \tag{41}$$

Since the system is designed such that all the poles of (34) are in the OLHP, one can write (23) at the steady state as

$$\dot{\mathbf{v}}_{\text{ref}}^{k,\text{ss}} = \mathbf{0} = -\left(\mathbf{L}^{k} + \mathbf{G}^{k}\right)\left(\mathbf{v}_{\text{ref}}^{k,\text{ss}} - \underline{\mathbf{v}}_{\text{ref}}^{k,\text{ss}}\right). \tag{42}$$

As mentioned in Section II, if the communication graph associated with $\mathbf{L}^{k}$ and $\mathbf{G}^{k}$ has, at least, one spanning tree and one pinned root node, the matrix $\mathbf{L}^{k} + \mathbf{G}^{k}$ is invertible and has positive real part for all the eigenvalues. Accordingly, (42) can be written as

$$\mathbf{v}_{\text{ref}}^{k,\text{ss}} - \underline{\mathbf{v}}_{\text{ref}}^{k,\text{ss}} = \left(\mathbf{L}^{k} + \mathbf{G}^{k}\right)\mathbf{0} = \mathbf{0} \tag{43}$$

which verifies the desired performance of the local tertiary controller at the steady state.

V. Experimental Verification

An experimental setup, with six energy sources, resistive loads, and transmission lines, is prototyped. As shown in Fig. 7, the controllable energy sources in the experimental setup are buck converters, connected to ac sources. The buck converter has two ac inputs, one for the main power and the other one for control circuits. The power input is provided by an autotransformer, which allows for change in input voltage, followed by an isolation transformer, which provides galvanic isolation. The output dc port [see Fig. 7(e)] is the point of connection of the

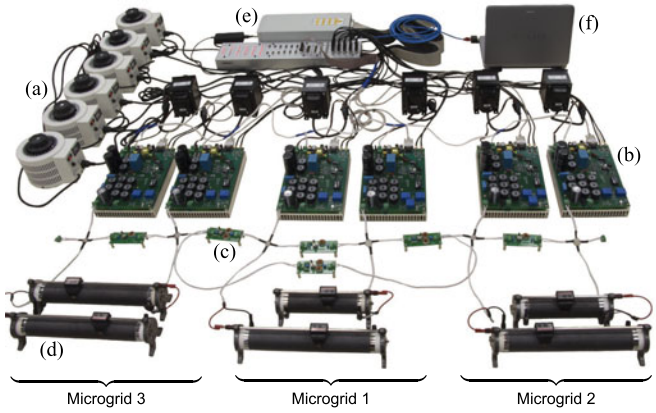

Fig. 8. Experimental setup for the cluster of three microgrids: (a) input ac sources, b) buck converters, (c) transmission lines, (d) resistive loads, (e) dSPACE DS1103 control boards, (f) programming and monitoring PC.

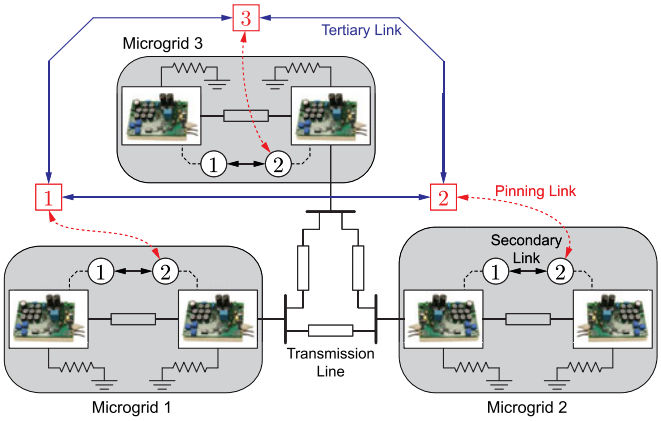

Fig. 9. Electrical connections and communication links in the setup of three microgrids.

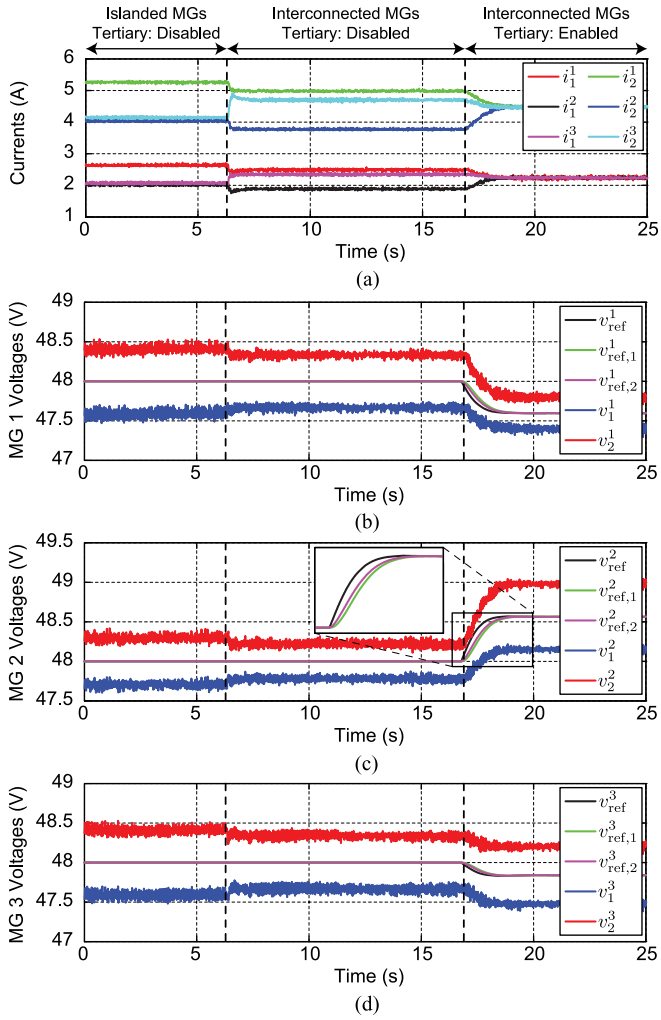

Fig. 10. Load sharing among microgrids when activating the proposed controller: (a) converter output currents, b) Microgrid 1 voltages, c) Microgrid 2 voltages, d) Microgrid 3 voltages.

source to loads/other sources. The input ac voltage is first rectified, using a diode bridge rectifier, and then passed through an *LC* filter to attenuate the ripples. At the next stage, the resulted dc voltage is chopped by two semiconductor switches and then passed through another *LC* filter to remove the harmonics from the output voltage of the converter.

To study different conditions, the controller performance is verified under two configurations. In the first configuration, a cluster of three microgrids are considered, each equipped with two buck converters. The second configuration includes two microgrids, each equipped with three buck converters. It should be noted that the proposed distributed control method is replicated in detail with separate modules in a single dSPACE control platform. In addition, in order to exactly replicate the behavior of communication links, the effects of delay and bandwidth limitation are also studied in the experiments.

A. Cluster of Three Microgrids

The cluster of three microgrids is shown in Fig. 8, where each microgrid consists of two buck converters and two loads. Fig. 9 shows the diagram of electrical connections and communication links for this cluster. Each microgrid has a point of connection (electrical bus), through which it can be connected to other microgrids. π-model transmission lines are used to connect the microgrids. The distribution lines within microgrids are all the same, but are different from the transmission lines used among microgrids. The line parameters are tabulated in the appendix. A switch is embedded on each transmission line to allow disconnecting. As seen in Fig. 9, every buck converter in the system has a local resistive load. Hereinafter, the converter i in microgrid k and its local load resistance are denoted by C_i^k and R_i^k, respectively. The parameters of the converters and the load resistances are given in the appendix. The controller performance is verified with the following four case studies grouped in two categories.

1) Controller Performance Validation: The three microgrids are set to be electrically disconnected from each other at the beginning. During this time, the tertiary and pinning links and, consequently, the global and local tertiary controllers are disabled. All converters consider the rated voltage of 48 V as their

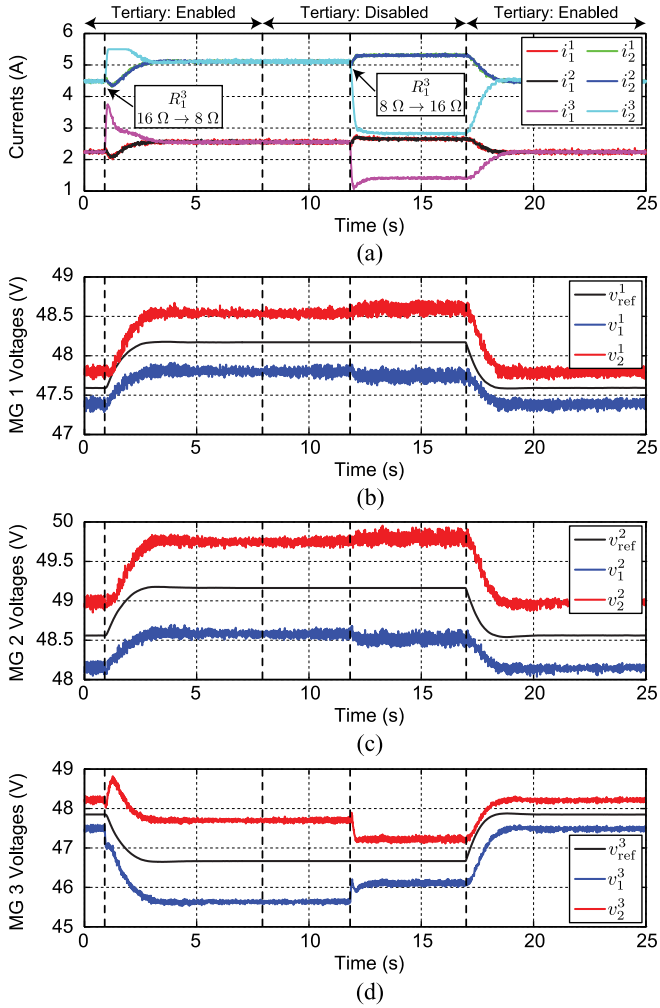

Fig. 11. Controller performance for a load change: (a) converter output currents, (b) Microgrid 1 voltages, (c) Microgrid 2 voltages, (d) Microgrid 3 voltages.

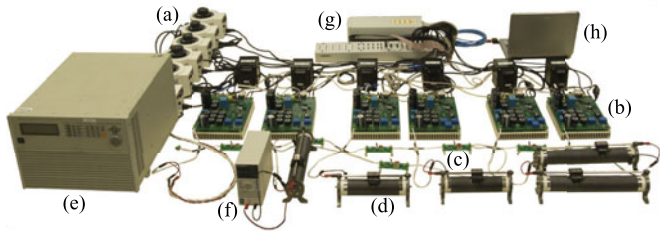

Fig. 12. Experimental setup for the cluster of three microgrids with constant power load: (a) input ac sources, (b) buck converters, (c) transmission lines, (d) resistive loads, (e) electronic load in constant power mode, (f) electronic load in constant resistor mode, (g) dSPACE DS1103 control boards, (h) programming and monitoring PC.

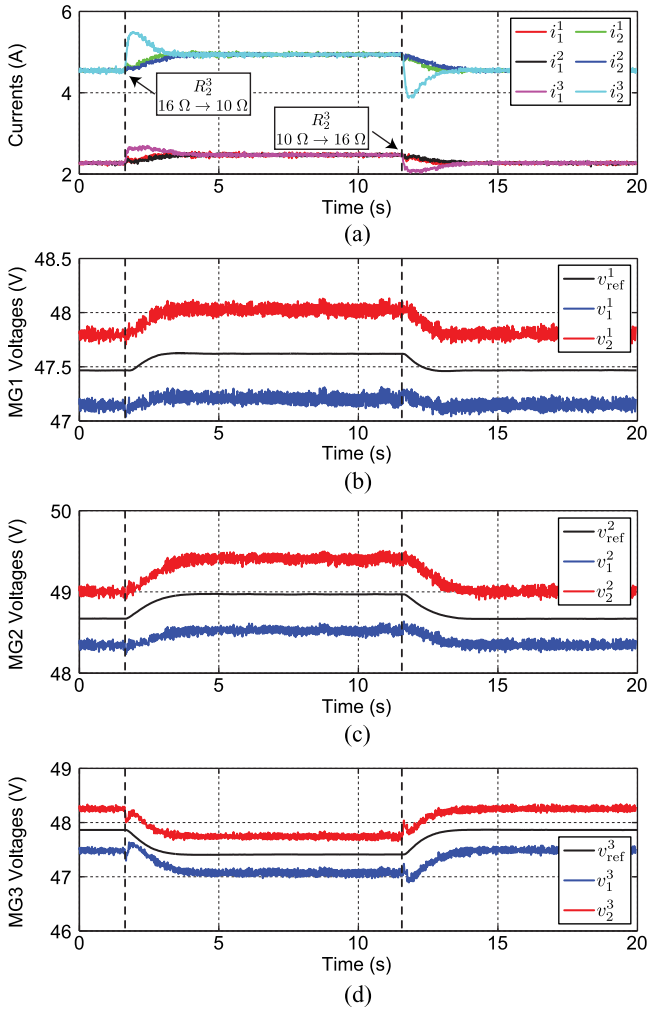

Fig. 13. Controller performance in presence of a nonlinear load: (a) converter output currents, (b) Microgrid 1 voltages, (c) Microgrid 2 voltages, (d) Microgrid 3 voltages.

reference value. As seen in Fig. 10(a), the secondary controller proportionally shares the load in each microgrid among the local sources, i.e., the current of converter C_2^k is twice the current of converter C_1^k, for all microgrids ($k = 1, 2, 3$). It should be noted that i_1^1 is higher than i_1^2 and i_1^3, and i_2^1 is higher than i_2^2 and i_2^3, which is due to less resistance in loads of Microgrid 1 compared to the other two. However, the output current of each converter is not exactly equal to its output voltage divided by its load resistance, which is its load current. In addition to load currents, currents of transmission lines, which are due to output voltage differences, also affect the output current of each converter. As shown in Fig. 10, the transmission lines between the microgrids become all connected at $t = 6.5$ s. At this time, the tertiary controllers are still disabled and the local reference voltage for each converter is still 48 V. The proportional load sharing within each individual microgrid is still established. The microgrids with less load (especially Microgrid 2), have less participation in the overall system load [see Fig. 10(a)]. At $t = 17$ s, the tertiary controllers are activated and the microgrids share the overall load and balance their currents by adjusting their local reference voltage v_{ref}^k [see Fig. 10(b)–(d)]. The local reference voltage at each converter follows the microgrid voltage set point for all microgrids, which is shown for Microgrid 2 in Fig. 10(c). As seen in Fig. 10(a), after activating the tertiary control, the per-unit currents of all six converters reach a consensus at 1.125 in the steady state, i.e., the current is 2.25 A for converters C_1^1, C_1^2, and C_1^3, and 4.5 A for converters C_2^1, C_2^2, and C_2^3.

Next, the effect of a load change on the controller performance is observed. As seen in Fig. 11, the system is initially

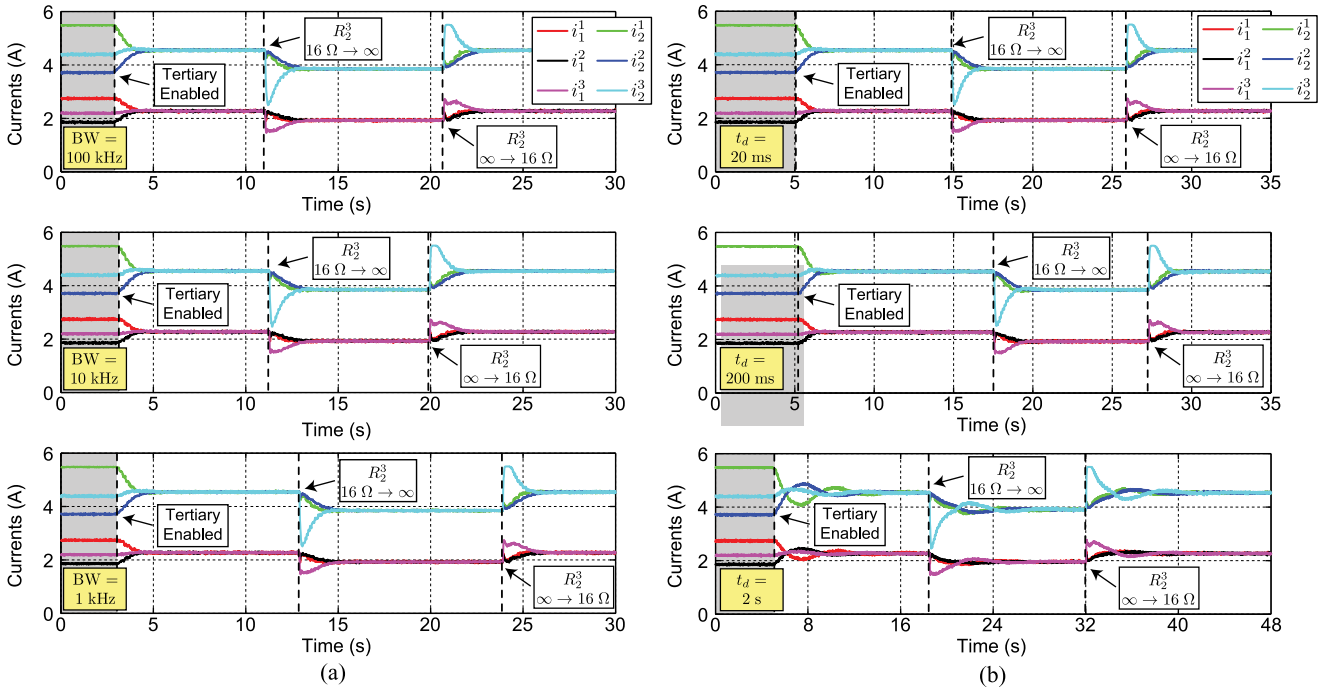

Fig. 14. Controller performance for a load change with different characteristics in communication links of tertiary controller: (a) different bandwidths, (b) different delay times.

operating under the proportional load sharing with the tertiary controllers in effect, when the load resistance R_1^3 is changed from 16 Ω to 8 Ω at $t = 0.9$ s. At this point, tertiary controllers change the microgrids' voltage set points and propagate them inside each microgrid [see Fig. 11(b)–(d)]. The cooperation of the controllers establishes the proportional load sharing after a short time [See Fig. 11(a)]. At $t = 7.9$ s, tertiary controllers are disabled; however, the voltage set point of each converter is not reset to the rated voltage and remains at the previous value. As seen in Fig. 11, the proportional load sharing is still established. The reason is that the microgrids' voltage set points have been previously set by the tertiary controllers, and the secondary controllers are still using those set points to balance the currents. The load R_1^3 is changed back to its initial value, 16 Ω, at $t = 11.8$ s. The proportional load sharing is clearly lost, for that the microgrid agents can no longer cooperate to adjust the set points for the new loading condition. At $t = 17$ s, the tertiary controllers are activated and the new voltage set points are generated and updated at each converter agent, which establishes the proportional load sharing again.

In the next study, an electronic load is added to the system to verify the controller performance in presence of nonlinear loads. As shown in Fig. 12, one of the resistive loads in the system, i.e., R_2^3 is replaced with an electronic load, set on constant power mode with 150 W. In addition, another electronic load is used in constant resistor mode to allow for load change [see Fig. 12(f)]. The results of this study are shown in Fig. 13, where one of the resistive loads, i.e., R_1^3 is changed from 16 Ω to 10 Ω at $t = 1.6$ s, while the tertiary controller is enabled. As seen in Fig. 13(a), proportional load sharing among microgrids, which is established before the load change, is established again after the load change with a short-time delay for dynamics of controllers, which accordingly change the voltage set points of microgrids [see Figs. 13(b)–(d)]. The resistive load is again changed back from 16 Ω to 10 Ω at $t = 11.5$ s, which causes the controllers to bring back all the voltages and currents to their initial values.

In the next two studies, the effect of change in communication links characteristics on controller performance is studied. For this purpose, the bandwidth and delay time of communication links of tertiary controller are changed. To replicate the effect of bandwidth of the links, a second-order filter with damping ratio $\zeta = 0.7$ is used. In order to see the effects of characteristics changes better, at the beginning of each experiment, the tertiary controller in disabled (see shaded parts in Fig. 14) and then becomes enabled. After settling the dynamics and establishing proportional load sharing, the resistive load R_2^3 is disconnected from the system, i.e., changed from 16 Ω to ∞. After establishing the new load sharing, the resistive load R_2^3 is connected to the system again. As shown in Fig. 14(a), a wide range of bandwidths is selected in the experiments, i.e., 100, 10, and 1 kHz, while the delay time is set to 20 ms. Comparing the results of Fig. 14(a), no significant difference can be seen in three of them. The controller performs well in load sharing for all different bandwidths. Since the bandwidth of the tertiary system is very low (much lower than the secondary and primary systems), decreasing the bandwidth of the links, even to 1 kHz does not affect controller performance. Three different delay times, i.e., 0.02, 0.2, and 2 s, are selected to study the delay time effect, while the bandwidth is set to 1 kHz [see Fig. 14(b)]. No significant difference can be observed between performances for delay times of 20 and 200 ms. In both cases, the proportional load sharing is established after short-time dynamics, preceding

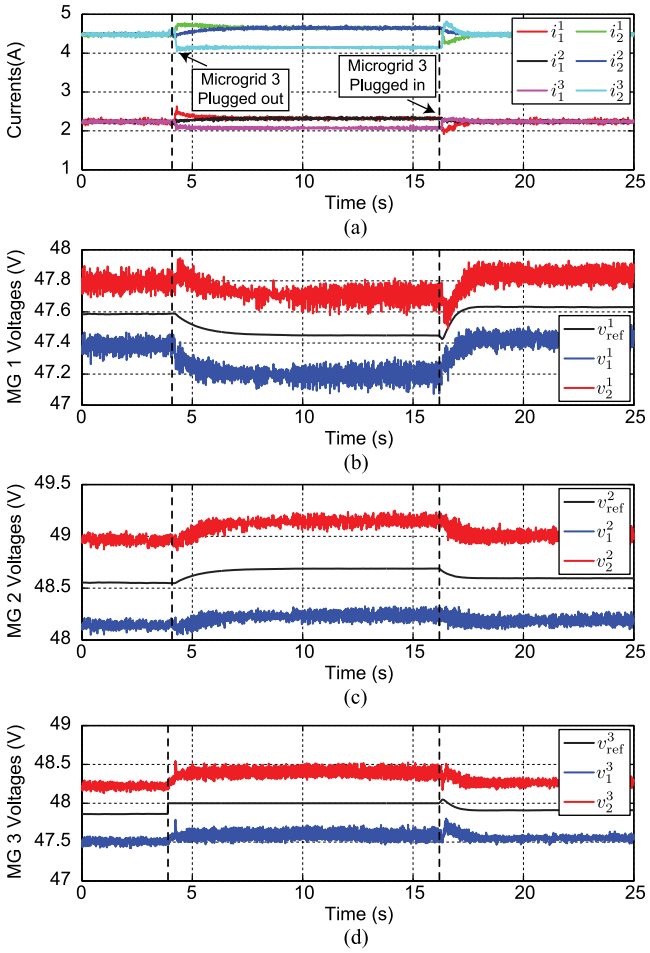

Fig. 15. Plug-and-play capability at the microgrid level: (a) converter output currents, (b) Microgrid 1 voltages, (c) Microgrid 2 voltages, (d) Microgrid 3 voltages.

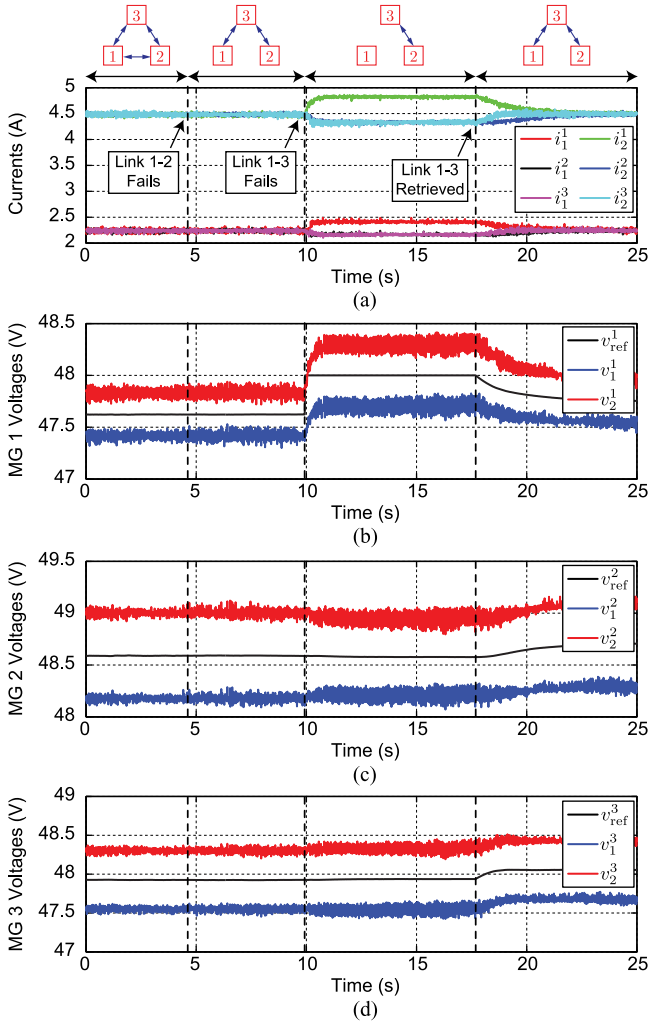

Fig. 16. Controller performance for a failure at the upper-level communication link: (a) converter output currents, (b) Microgrid 1 voltages, (c) Microgrid 2 voltages, (d) Microgrid 3 voltages.

each change in the system. However, in the case of $t_d = 2$ s, the dynamics take much longer to decay. However, the overshoots/undershoots remain intact and the controller performs well at the steady state. In overall, it can be concluded that the controller performance has immunity to delay times as long as 200 ms and bandwidths as low as 1 kHz. Therefore, common communication protocols, such as WiFi and UWB, are possible choices. Interested readers are encouraged to read more details on communication links characteristics in distributed systems in [45], [49], [50].

2) Fault Tolerance: The plug-and-play capability of the proposed controller is studied, where one of the microgrids is plugged out and then back in. As shown in Fig. 15, the system is operating under normal conditions at the nominal values until $t = 4.05$ s, when the Microgrid 3 is plugged out by disconnecting the transmission lines between Microgrid 3 and other microgrids and deactivating its global tertiary controller. Consequently, the voltage set point for Microgrid 3 is reset to 48 V [see Fig. 15(d)]. It is noteworthy that the other two microgrid agents and the tertiary link between them is still active, which provide cooperative load sharing between Microgrids 1 and 2. Fig. 15(a) reports an excellent current sharing between Microgrids 1 and 2, while Microgrid 3 is disconnected from the two and has an internal load sharing mechanism. Then, Microgrid 3 is plugged back at $t = 16.2$ s, when the transmission lines are connected again and all communication links are activated such that the tertiary control system updates the set points to share the load. As reported in Fig. 15, the voltages and currents finally return to their initial values.

Next, a failure in tertiary links is studied. As shown in Fig. 9, the tertiary graph is a fully connected graph, which has three links between the three microgrid agents. The microgrids are operating under normal conditions until $t = 4.6$ s, when Link 1–2 of the tertiary graph is failed. As reported in Fig. 16, no change is observed in microgrid currents or voltages. This is because the tertiary graph is still connected, which shows system resiliency in the case of a single-link failure. It is further shown that, when the tertiary graph loses its connectivity, the proportional load sharing is lost. As seen in Fig. 16, Link 1–3 fails at $t = 9.9$ s, which separates the node 1 from the rest of the graph.

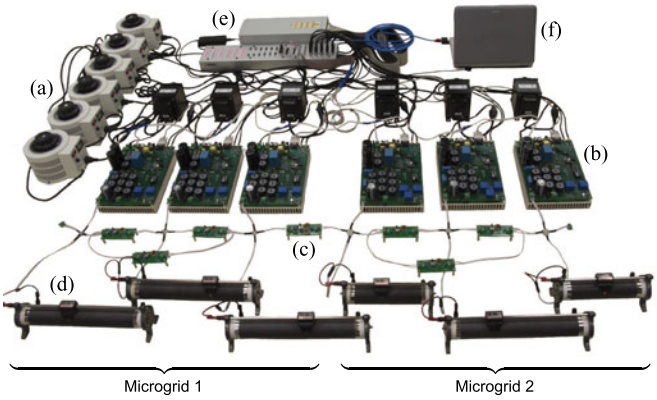

Fig. 17. Experimental setup for the cluster of two microgrids: (a) input ac sources, (b) buck converters, (c) transmission lines, (d) resistive loads, (e) dSPACE DS1103 control boards, (f) programming and monitoring PC.

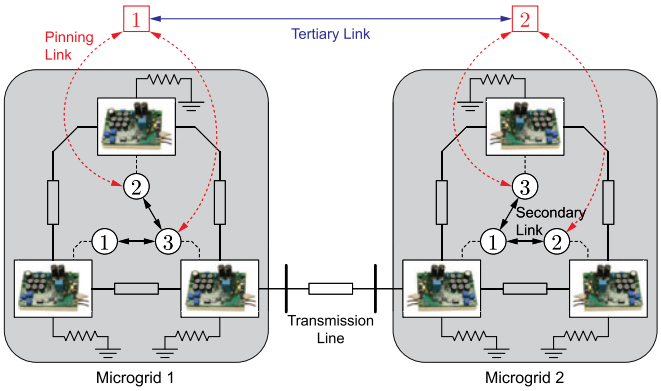

Fig. 18. Electrical connections and communication links in the setup of two microgrids.

Once it has no communication with other microgrid agents, the local voltage set point of Microgrid 1, $v^1_{\rm ref}$ is set to 48 V [see Fig. 16(b)]. Fig. 16(a) reports an excellent current sharing between Microgrids 2 and 3, while Microgrid 1 shares the local load among its own converters proportionally. Finally, one of the failed links is retrieved at $t = 17.7$ s, which establishes the connectivity of the tertiary graph and brings the system back to the normal operation.

B. Cluster of Two Microgrids

In this section, the system is reconfigured to build up two microgrids, each consists of three buck converters and three loads. (see Fig. 17). The electrical connections and communication links are shown in Fig. 18. The transmission lines have the same parameters as previously given in Table I. Converters' parameters are tabulated in the appendix.

Fig. 19 shows the bode diagram of different voltage and current transfer functions, given in (31), for Microgrid 1 in this configuration. Fig. 19(a) exhibits the transfer functions from the voltage set point $V^1_{\rm ref}$, to the output voltages of the three converters in Microgrid 1, V^1_i for $i = 1$ to 3. The voltage transfer function $\frac{V^1_i}{V^1_{\rm ref}}$ is the ith entry of transfer function matrix $\mathbf{H}^1_V$. As seen in Fig. 19(a), all three output voltages demonstrate the same response to this excitation at low frequencies, i.e., the magnitude of all voltage transfer functions is equal to 1 and their phases are equal to zero for $f < 3$ Hz. This means that the average output voltage is also equal to the common set point value of all three converters. Similarly, Fig. 19(b) shows the transfer functions from the voltage set point $V^1_{\rm ref}$, to the output currents of the three converters in Microgrid 1, I^1_i for $i = 1$ to 3, where the current transfer function $\frac{I^1_i}{V^1_{\rm ref}}$ is the ith entry of transfer function matrix $\mathbf{H}^1_I$. As seen in Fig. 19(a), at low frequencies, Converter 2 has the response magnitude equal to 0.0375 and the other two converters, which have rated currents as twice as that of Converter 2, have the response magnitude equal to 0.075. All the phases are also equal to zero at low frequencies. Such a response expresses the proportional load sharing at low frequencies, which is provided by the secondary and primary controllers.

Next, a study is run to verify the plug-and-play capability of the proposed controller at the converter level. As shown in Fig. 20, the two microgrids are operating under normal conditions in the beginning. Fig. 20(a) confirms excellent load sharing in the case of two microgrids. The per-unit currents of all the six converters have reached the consensus at 0.716, i.e., the output current is 2.15 A for converters C^1_2 and C^2_2, which have the rated current of 3 A, and is 4.3 A for the rest of the converters, which have the rated current of 6 A. As seen in Fig. 20, converter 2 fails at $t = 5.4$ s and its current drops to zero. The tertiary control system adjusts the reference voltages to establish load sharing among the five remaining converters. As seen in Fig. 20(b) and (c), the voltage set points of Microgrid 1 and 2 decrease and increase, respectively, which cause Microgrid 2 to provide more power than Microgrid 1. Accordingly, the per-unit currents of all active converters reach consensus at 1.175, i.e., 2.35 A for converter C^2_2, and 4.7 A for the rest of active converters. At $t = 15$ s, converter 2 is retrieved. The tertiary control system again adjusts the voltage set points, which causes all voltages and currents to return to their initial values.

Finally, the failure of the pinning communication link is studied. As shown in Fig. 18, two converter agents are pinned for every microgrid, which are converter agents 2 and 3 for Microgrid 1. As seen in Fig. 21, the system is running under normal conditions, until $t = 6$ s, when the pinning link of converter 2 in Microgrid 1 fails. It should be noted that a failure in the pinning gain communication has two effects: 1) the microgrid agent cannot transmit the local voltage reference to the previously pinned converter agent; 2) the previously pinned converter agent cannot transmit its per-unit current (i.e., loading ratio) to the microgrid agent, upon which the microgrid agent decreases the number of pinned converter agents in the averaging process of (6). It can be seen that the failure in the first pinning communication link does not have any effect on the converter voltages and currents, because converter agent 3 in Microgrid 1 still remains pinned, and the system can continue its performance with only one pinned converter agent.

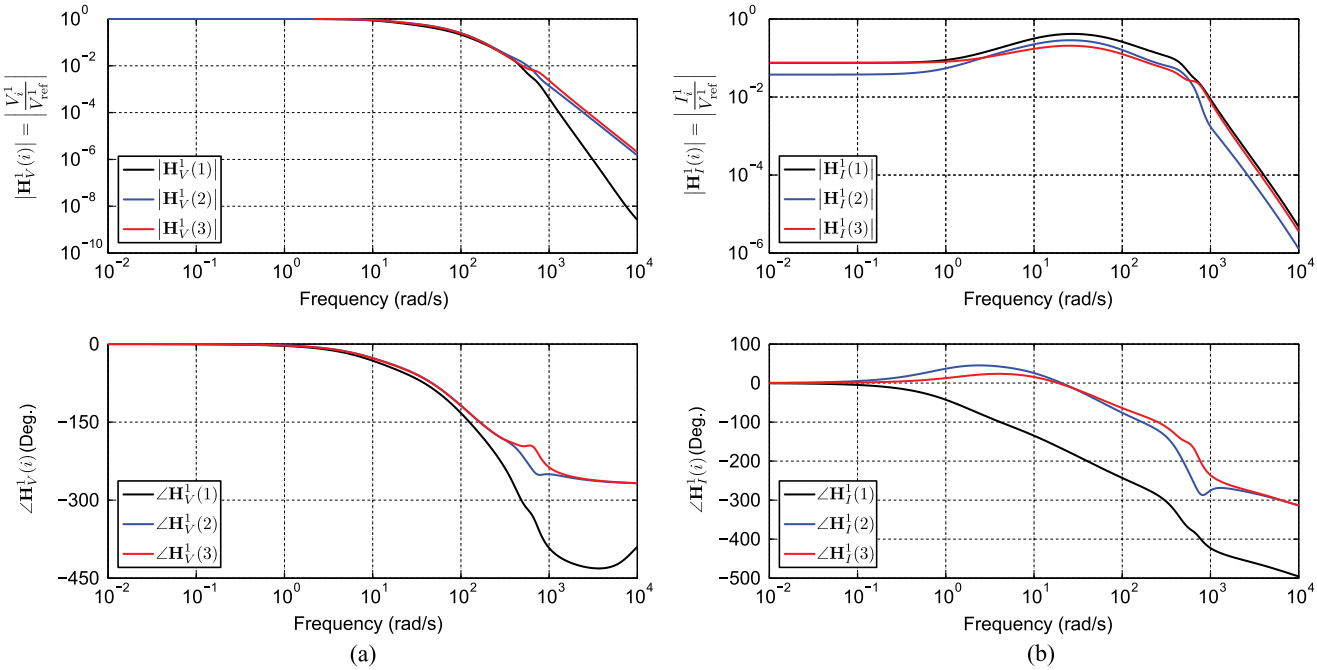

Fig. 19. Microgrid 1 voltage and current transfer functions: (a) From voltage set point $V^1_{\rm ref}$, to the output voltages of three converters V^1_i. (b) From voltage set point $V^1_{\rm ref}$ to the output currents of three converters I^1_i.

Later, at $t = 9$ s, the other pinning link in Microgrid 1 fails, which causes all converter agents in Microgrid 1 to become unpinned. Having no connection with the leader, all of the converter agents in Microgrid 1 can only communicate with each other and cannot update their local reference voltage from their leader. However, the converter agents cannot detect that all of the pinning links have failed. Accordingly, they will continue to keep their local reference on the previous set point, at which they had a consensus. On the other hand, since Microgrid agent 1 is disconnected from its corresponding converter agents, it becomes isolated, and automatically its communication link to other microgrid agents (in this case, Microgrid agent 2 is disabled. Accordingly, both Microgrid agents are isolated and reset their voltage set point to 48 V, which is propagated to the converters of Microgrid 2 only. Fig. 21(b) and (c) shows that the average of voltages in Microgrid 1 is kept at the previous value, while the average of voltages in Microgrid 2 is increased to 48 V after the second failure. In addition, the proportional load sharing is established in each microgrid individually, but not for the overall system [see Fig. 21(a)]. At $t = 18$ s, one of the failed pinning links is retrieved, which automatically activates the tertiary link between the two microgrids and brings the system back to its normal operation.

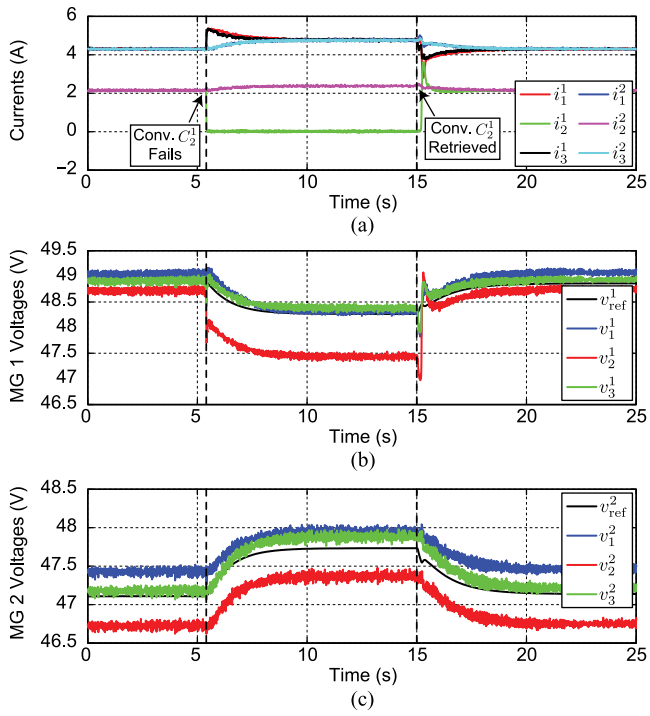

Fig. 20. Plug-and-play capability at the converter level: (a) Converter output currents, (b) Microgrid 1 voltages, (c) Microgrid 2 voltages.

VI. Conclusion

A distributed control method is proposed for load sharing within a microgrid cluster. The proposed method works at the tertiary control level, in a hierarchical control structure, and operates at two levels. At the global level (among microgrids), the voltage set point of each microgrid is generated based on the loading data among the microgrids. At the local level (within each microgrid), the generated set points are propagated across the converters in each microgrid and will be used by the secondary control level. The proposed solution works with the

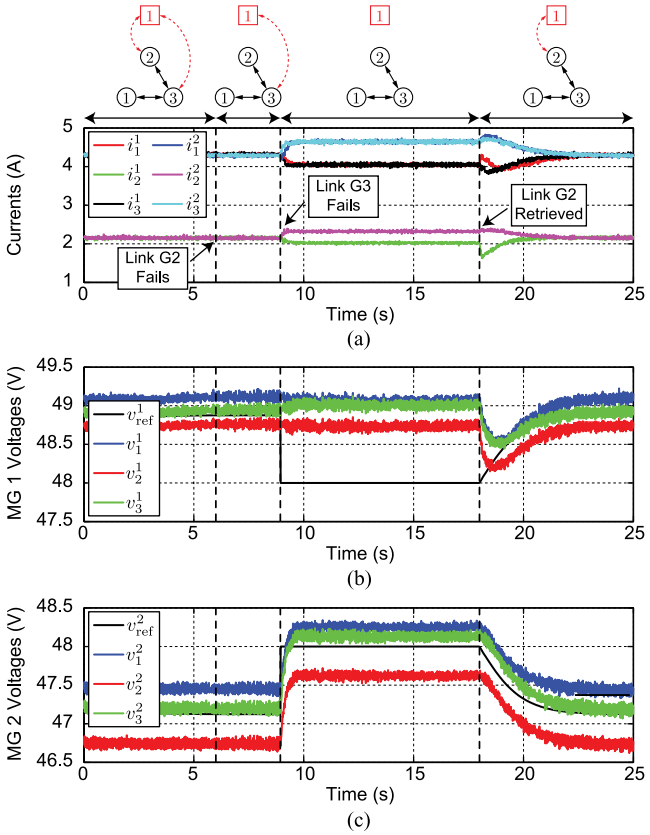

Fig. 21. Controller performance considering failures in pinning links: (a) Converter output currents, (b) Microgrid 1 voltages, (c) Microgrid 2 voltages.

TABLE I
PARAMETERS OF INTERNAL (WITHIN A MICROGRID) AND EXTERNAL (AMONG MICROGRIDS) TRANSMISSION LINES

Transmission Line	R (Ω)	L (μH)	C (nF)
Internal	0.5	56	22
External	1	112	44

distributed secondary control system to benefit from its communication structure in propagating voltage set points. It does not require *a priori* knowledge of the number of microgrids in the cluster and, therefore, provides a plug-and-play capability. Experimental results verify the controller performance in load sharing among microgrids, as well as its physical- and cyber-fault resiliency.

APPENDIX

Transmission line parameters in the experimental setup are given in Table I. The parameters of buck converters for the two different configurations are tabulated in Tables II and III, respectively. For the cluster of three microgrids, the adjacency matrix is

TABLE II
PARAMETERS OF BUCK CONVERTERS IN THE CLUSTER OF THREE MICROGRIDS

Converter	v_{in} (V)	L_{out} (mH)	C_{out} (mF)	I_{rated} (A)	R (Ω)
C_1^1	100	3.11	2.14	3	12
C_2^1	100	3.1	2.15	6	12
C_1^2	80	3.09	2.07	3	16
C_2^2	100	3.12	2.19	6	16
C_1^3	100	3.1	2.1	3	16
C_2^3	80	3.11	2.12	6	16

TABLE III
PARAMETERS OF BUCK CONVERTERS IN THE CLUSTER OF TWO MICROGRIDS

Converter	v_{in} (V)	L_{out} (mH)	C_{out} (mF)	I_{rated} (A)	R (Ω)
C_1^1	100	3.1	2.1	6	16
C_2^1	80	3.11	2.12	3	16
C_3^1	100	3.11	2.14	6	16
C_1^2	100	3.1	2.15	6	12
C_2^2	80	3.09	2.07	3	12
C_3^2	100	3.12	2.19	6	12

matrix is

$$\mathbf{A} = \begin{bmatrix} 0 & 2 & 2 \\ 2 & 0 & 2 \\ 2 & 2 & 0 \end{bmatrix}. \tag{44}$$

and the pinning gain matrices are

$$\mathbf{G}^1 = \begin{bmatrix} 0 & 0 \\ 0 & 10 \end{bmatrix}, \quad \mathbf{G}^2 = \begin{bmatrix} 0 & 0 \\ 0 & 8 \end{bmatrix}, \quad \mathbf{G}^3 = \begin{bmatrix} 0 & 0 \\ 0 & 9 \end{bmatrix}. \tag{45}$$

The controller transfer-functions are $G_c^k(s) = \frac{1}{s}$ for $k = 1, 2, 3$. For the cluster of two microgrids, the adjacency matrix is

$$\mathbf{A} = \begin{bmatrix} 0 & 3 \\ 3 & 0 \end{bmatrix} \tag{46}$$

and the pinning gain matrices are

$$\mathbf{G}^1 = \begin{bmatrix} 0 & 0 & 0 \\ 0 & 10 & 0 \\ 0 & 0 & 10 \end{bmatrix}, \quad \mathbf{G}^2 = \begin{bmatrix} 0 & 0 & 0 \\ 0 & 8 & 0 \\ 0 & 0 & 8 \end{bmatrix}. \tag{47}$$

The controller transfer-functions are $G_c^k(s) = \frac{1}{s}$ for $k = 1, 2$.

REFERENCES

[1] D. Chen and L. Xu, "Autonomous dc voltage control of a dc microgrid with multiple slack terminals," *IEEE Trans. Power Syst.*, vol. 27, no. 4, pp. 1897–1905, Nov. 2012.
[2] M. Datta, T. Senjyu, A. Yona, T. Funabashi, and C. H. Kim, "A frequency-control approach by photovoltaic generator in a PV-diesel hybrid power system," *IEEE Trans. Energy Convers.*, vol. 26, no. 2, pp. 559–571, Jun. 2011.
[3] S. Teleke, M. E. Baran, A. Q. Huang, S. Bhattacharya, and L. Anderson, "Control strategies for battery energy storage for wind farm dispatching," *IEEE Trans. Energy Convers.*, vol. 24, no. 3, pp. 725–732, Sep. 2009.
[4] J. M. Guerrero, J. C. Vasquez, J. Matas, L. G. de Vicuña, and M. Castilla, "Hierarchical control of droop-controlled ac and dc microgrids—A general approach toward standardization," *IEEE Trans. Ind. Electron.*, vol. 58, no. 1, pp. 158–172, Jan. 2011.

[5] R. Majumder, B. Chaudhuri, A. Ghosh, R. Majumder, G. Ledwich, and F. Zare, "Improvement of stability and load sharing in an autonomous microgrid using supplementary droop control loop," *IEEE Trans. Power Syst.*, vol. 25, no. 2, pp. 796–808, May 2010.

[6] H. Kakigano, Y. Miura, and T. Ise, "Distribution voltage control for dc microgrids using fuzzy control and gain-scheduling technique," *IEEE Trans. Power Electron.* vol. 28, no. 5, pp. 2246–2258, May 2013.

[7] D. Salomonsson, L. Soder, and A. Sannino, "An adaptive control system for a dc microgrid for data centers," *IEEE Trans. Ind. Appl.*, vol. 44, no. 6, pp. 1910–1917, Nov./Dec. 2008.

[8] A. Kwasinski, "Quantitative evaluation of dc microgrids availability: Effects of system architecture and converter topology design choices," *IEEE Trans. Power Electron.*, vol. 26, no. 3, pp. 835–851, Mar. 2011.

[9] Y. C. Chang and C. M. Liaw, "Establishment of a switched-reluctance generator-based common dc microgrid system," *IEEE Trans. Power Electron.*, vol. 26, no. 9, pp. 2512–2527, Sep. 2011.

[10] Y. Gu, X. Xiang, W. Li, and X. He, "Mode-adaptive decentralized control for renewable dc microgrid with enhanced reliability and flexibility," *IEEE Trans. Power Electron.*, vol. 29, no. 9, pp. 5072–5080, Sep. 2014.

[11] H. Kakigano, Y. Miura, and T. Ise, "Low-voltage bipolar-type dc microgrid for super high quality distribution," *IEEE Trans. Power Electron.*, vol. 25, no. 12, pp. 3066–3075, Dec. 2010.

[12] Y. K. Chen, Y. C. Wu, C. C. Song, and Y. S. Chen, "Design and implementation of energy management system with fuzzy control for dc microgrid systems," *IEEE Trans. Power Electron.*, vol. 28, no. 4, pp. 1563–1570, Dec. 2013.

[13] P. C. Loh, D. Li, Y. K. Chai, and F. Blaabjerg, "Autonomous operation of hybrid microgrid with ac and dc subgrids," *IEEE Trans. Power Electron.*, vol. 28, no. 5, pp. 2214–2223, May 2013.

[14] S. R. Huddy and J. D. Skufca, "Amplitude death solutions for stabilization of dc microgrids with instantaneous constant-power loads," *IEEE Trans. Power Electron.*, vol. 28, no. 1, pp. 247–253, Jan. 2013.

[15] N. Bottrell, M. Prodanovic, and T. C. Green, "Dynamic stability of a microgrid with an active load," *IEEE Trans. Power Electron.*, vol. 28, no. 11, pp. 5107–5119, Nov. 2013.

[16] Z. Jiang and X. Yu, "Hybrid dc- and ac-linked microgrids: Towards integration of distributed energy resources," in *Proc. IEEE Conf. Global Sustain. Energy Infrastruct.*, 2008, pp. 1–8.

[17] A. Kwasinski and C. N. Onwuchekwa, "Dynamic behavior and stabilization of dc microgrids with instantaneous constant-power loads," *IEEE Trans. Power Electron.*, vol. 26, no. 3, pp. 822–834, Mar. 2011.

[18] R. S. Balog, W. Weaver, and P. T. Krein, "The load as an energy asset in a distributed dc smartgrid architecture," *IEEE Trans. Smart Grid*, vol. 3, no. 1, pp. 253–260, Mar. 2012.

[19] V. Nasirian, S. Moayedi, A. Davoudi, and F. Lewis, "Distributed cooperative control of dc microgrids," *IEEE Trans. Power Electron.*, vol. 30, no. 4, pp. 2288–2303, Apr. 2015.

[20] A. Bidram and A. Davoudi, "Hierarchical structure of microgrids control system," *IEEE Trans. Smart Grid*, vol. 3, no. 4, pp. 1963–1976, Dec. 2012.

[21] F. Katiraei, R. Iravani, N. Hatziargyriou, and A. Dimeas, "Microgrids management," *IEEE Power Energy Mag.*, vol. 6, no. 3, pp. 54–65, May/Jun. 2008.

[22] A. Mehrizi-Sani and R. Iravani, "Potential-function based control of a microgrid in islanded and grid-connected models," *IEEE Trans. Power Syst.*, vol. 25, no. 4, pp. 1883–1891, Nov. 2010.

[23] J. C. Vasquez, J. M. Guerrero, J. Miret, M. Castilla, and L. de Vicuña, "Hierarchical control of intelligent microgrids," *IEEE Ind. Electron. Mag.*, vol. 4, no. 4, pp. 23–29, Dec. 2010.

[24] L. Xu and D. Chen, "Control and operation of a dc microgrid with variable generation and energy storage," *IEEE Trans. Power Del.*, vol. 26, no. 4, pp. 2513–2522, Oct. 2011.

[25] H. Kanchev, D. Lu, F. Colas, V. Lazarov, and B. Francois, "Energy management and operational planning of a microgrid with a pv-based active generator for smart grid applications," *IEEE Trans. Ind. Electron.*, vol. 58, no. 10, pp. 4583–4592, Oct. 2011.

[26] P. Huang, W. Xiao, and M. S. E. Moursi, "A practical load sharing control strategy for dc microgrids and dc supplied houses," in *Proc. 39th Annu. IEEE Ind. Electron. Soc. Conf.*, Nov. 2013, pp. 7124–7128.

[27] V. Nasirian, A. Davoudi, F. L. Lewis, and J. M. Guerrero, "Distributed adaptive droop control for dc distribution systems," *IEEE Trans. Energy Convers.*, vol. 29, no. 4, pp. 944–956, Dec. 2014.

[28] H. Behjati, A. Davoudi, and F. Lewis, "Modular dc-dc converters on graphs: Cooperative control," *IEEE Trans. Power Electron.*, vol. 29, no. 12, pp. 6725–6741, Dec. 2014.

[29] P. J. Grbovic, "Master/slave control of input-series- and output-parallel-connected converters: Concept for low-cost high-voltage auxiliary power supplies," *IEEE Trans. Power Electron.*, vol. 24, no. 2, pp. 316–328, Feb. 2009.

[30] S. Moayedi, V. Nasirian, F. Lewis, and A. Davoudi, "Team-oriented load sharing in parallel dc-dc converters," *IEEE Trans. Ind. Appl.*, vol. 51, no. 1, pp. 479–490, Jan./Feb. 2015.

[31] Q. Shafiee, T. Dragicevic, J. C. Vasquez, and J. M. Guerrero, "Modeling, stability analysis and active stabilization of multiple dc-microgrid clusters," in *Proc. IEEE Int. Energy Conf.*, May 2014, pp. 1284–1290.

[32] L. Che and M. Shahidehpour, "DC microgrids: Econic operation and enhancement of resilience by hierarchical control," *IEEE Trans. Smart Grid*, vol. 5, no. 5, pp. 2517–2526, Sep. 2014.

[33] I. U. Nutkani, W. Peng, P. C. Loh, and F. Blaabjerg, "Autonomous economic operation of grid connected dc microgrid," in *Proc. IEEE 5th Int. Symp. Power Electron. Dist. Gen. Syst.*, Jun. 2014, pp. 1–5.

[34] L. Meng, T. Dragicevic, J. M. Guerrero, and J. C. Vasquez, "Dynamic consensus algorithm based distributed global efficiency optimization of a droop controlled dc microgrid," in *Proc. IEEE Int. Energy Conf.*, May 2014, pp. 1276–1283.

[35] X. Yu, X. She, and A. Huang, "Hierarchical power management for dc microgrid in islanding mode and solid state transformer enabled mode," in *Proc. 39th Annu. IEEE Ind. Electron. Soc. Conf.*, Nov. 2013, pp. 1656–1661.

[36] L. Zhang, T. Wu, Y. Xing, K. Sun, and J. M. Guerrero, "Power control of dc microgrid using dc bus signaling," in *Proc. 26th IEEE Annu. Appl. Power Electron. Conf. Expo.*, Mar. 2011, pp. 1926–2932.

[37] T. Zhou and B. Francois, "Energy management and power control of a hybrid active wind generator for distributed power generation and grid integration," *IEEE Trans. Ind. Electron.*, vol. 58, no. 1, pp. 95–104, Jan. 2011.

[38] A. Khorsandi, M. Ashourloo, and H. Mokhtari, "A decentralized control method for a low-voltage dc microgrid," *IEEE Trans. Energy Convers.*, vol. 29, no. 4, pp. 793–801, Dec. 2014.

[39] J. Schonberger, R. Duke, and S. D. Round, "DC-bus signaling: A distributed control strategy for a hybrid renewable nanogrid," *IEEE Trans. Ind. Electron.*, vol. 53, no. 5, pp. 1453–1460, Oct. 2006.

[40] D. Chen, L. Xu, and L. Yao, "DC voltage variation based autonomous control of dc microgrids," *IEEE Trans. Power Del.*, vol. 28, no. 2, pp. 637–648, Apr. 2013.

[41] A. Bidram, F. L. Lewis, and A. Davoudi, "Distributed control systems for small-scale power networks: Using multiagent cooperative control theory," *IEEE Control Syst.*, vol. 34, no. 6, pp. 56–77, Dec. 2014.

[42] V. Nasirian, Q. Shafiee, J. M. Guerrero, F. L. Lewis, and A. Davoudi, "Droop-free distributed control for ac microgrids," 2015, doi: 10.1109/TPEL.2015.2414457.

[43] A. Bidram, A. Davoudi, and F. L. Lewis, "A multiobjective distributed control framework for islanded ac microgrids," *IEEE Trans. Ind. Informat.*, vol. 10, no. 3, pp. 1785–1798, Aug. 2014.

[44] Z. Qu, *Cooperative Control of Dynamical Systems: Applications to Autonomous Vehicles*. New York, NY, USA: Springer-Verlag, 2009.

[45] R. Olfati-Saber and R. M. Murray, "Consensus problems in networks of agents with switching topology and time-delays," *IEEE Trans. Autom. Control*, vol. 49, no. 9, pp. 1520–1533, Sep. 2004.

[46] S. Moayedi and A. Davoudi, "Distributed cooperative load sharing in parallel dc-dc converters," in *Proc. 29th IEEE Annu. Appl. Power Electron. Conf. and Expo.*, Mar. 2014, pp. 2907–2912.

[47] H. Xin, Z. Lu, Z. Z. Qu, D. Gan, and D. Qi, "Cooperative control strategy for multiple photovoltaic generators in distribution networks," *IET Control Theory Applications*, vol. 5, no. 14, pp. 1617–1629, Sep. 2011.

[48] S. Anand, B. G. Fernandes, and J. M. Guerrero, "Distributed control to ensure proportional load sharing and improve voltage regulation in low-voltage dc microgrids," *IEEE Trans. Power Electron.*, vol. 28, no. 4, pp. 1900–1913, Apr. 2013.

[49] N. Amelina and A. Fradkov, "Consensus problem in stochastic network systems with switched topology, noise and delay," in *Proc. 12th IEEE Int. Conf. Netw.*, Jan. 2013, pp. 118–124.

[50] S. Kar and J. M. F. Moura, "Distributed consensus algorithms in sensor networks with imperfect communication: Link failures and channel noise," *IEEE Trans. Signal Process.*, vol. 57, no. 1, pp. 355–369, Jan. 2009.

Seyedali Moayedi (S'12) received the B.Sc. and M.Sc. degrees in electrical engineering from the Sharif University of technology, Tehran, Iran, in 2007 and 2009, respectively. He is currently working toward the Ph.D. degree at the University of Texas at Arlington, Arlington, TX, USA.

His research interests include modeling and control of power electronics, electric drive systems, and distributed control systems.

Ali Davoudi (S'04–M'11) received the Ph.D. degree in electrical and computer engineering from the University of Illinois, Urbana-Champaign, Champaign, IL, USA, in 2010.

He is currently an Assistant Professor at the Electrical Engineering Department, University of Texas-Arlington, Arlington, TX, USA. He was with Solar Bridge Technologies, Texas Instruments Inc., and Royal Philips Electronics. His research interests include various aspects of modeling and control of power electronics and finite-inertia power systems.

Dr. Davoudi is an Associate Editor for the IEEE TRANSACTIONS ON INDUSTRY APPLICATIONS, the IEEE TRANSACTIONS ON ENERGY CONVERSION, and the IEEE TRANSACTIONS ON TRANSPORTATION ELECTRIFICATION.